About two-phase flow distribution improvement in the header of a simplified evaporator A multi-factorial study with the help of a Design of Experiment technique

Lecardonnel, Aude; Falsetti, Chiara; Tempesti, Claretta; Laboureur, Delphine

DOI
10.1016/j.applthermaleng.2025.128034

Publication date
2025

Document Version
Final published version

Published in
Applied Thermal Engineering

Applied Thermal Engineering 279 (2025) 128034

Contents lists available at ScienceDirect

Applied Thermal Engineering

journal homepage: www.elsevier.com/locate/ate

Research Paper

About two-phase flow distribution improvement in the header of a simplified evaporator: A multi-factorial study with the help of a Design of Experiment technique

Aude Lecardonnel [a,b,*], Chiara Falsetti [b], Claretta Tempesti [a], Delphine Laboureur [a]

[a] Von Karman Institute for Fluid dynamics, Chaussee de Waterloo 72, Rhode-Saint-Genese, 1640, Belgium
[b] Propulsion and Power, Delft University of Technology, Kluyverweg 1, Delft, 2629HS, The Netherlands

ARTICLE INFO

Keywords:
Evaporator design
Two-phase flow
Maldistribution
Design of Experiment

ABSTRACT

This study experimentally investigates the combined impact of several parameters on the two-phase flow distribution in an evaporator header for an air/water mixture, in flow pattern similarity with a low Global Warming Potential refrigerant. The test were performed at isothermal conditions under the assumption that phase change is negligible in an evaporator header. The water and air flow rates were varied and three inlet qualities were targeted ($x = 0.04, 0.1$ and 0.25). Total mass fluxes G ranging from 42 kg/(s m^2) to 513 kg/(s m^2) were covered. The impact of the fluid properties on the flow patterns was preliminary and theoretically evaluated by means of flow maps for all pipe directions: horizontal, vertical upward and vertical downward. A rectangular header connected to eight parallel channels of internal diameter (I.D.) of 10 mm was used to mimic an evaporator. Four header and channels orientations were investigated. The inlet position and the diameter of the feeding tube (23 mm or 56 mm) could be changed as well as the channels intrusion inside the header height. A flow pattern breaking device, also called splashing grid, was also tested at the inlet of the header. A Design Of Experiment (DOE) technique was used to build an optimized test matrix ensuring that the impact of each parameter individually as well as their combinations could be assessed in a balanced manner and within a minimum amount of tests. Forty-eight tests were needed. The standard deviation of the water flow distribution among the channels is set as comparative variable. Based on the experimental results, a ranking of the most influential parameters was established. The study highlights that the orientation of the header and channels is the most significant parameter impacting the flow distribution, followed the tube inlet position. The combined influence of the inlet tube position and diameter, the tube intrusion and the presence/absence of the splashing grid is evaluated for each of the four orientations. Based on these conclusions, design rules were established for each header and channel orientation. The findings of this research represent a significant advancement in the field and can serve as a foundation for greatly improving flow distribution within evaporators, thereby enhancing their thermal performance.

1. Introduction

The improvement of the performances of Vapor Cycle Systems (VCS) has been the subject of decades of research. Indeed, these closed loop systems that use refrigerants as working fluids are present in numerous fields for cooling requirement such as the pharmaceutical industry, the aeronautical and the automotive sectors, the building and food industries [1]. Due to their massive use, an even small efficiency enhancement would lead to a significant amount of power saved. One way to enhance the efficiency of VCS is to optimize its components, such as the evaporator. Consequently, evaporators are continuously under research for improvement. One straightforward way to intensify their performances is to improve the refrigerant flow distribution among the evaporator channels. Indeed, at the inlet of this specific type of heat exchanger, the refrigerant is mostly found in a liquid/gas two-phase state, which makes the distribution much harder to predict than for a single phase flow. However, a non uniform distribution among channels can drop the evaporator performances by 13% [2] and up to 30% in the worst cases [3]. Thereby, extensive scientific endeavor has

* Corresponding author at: Von Karman Institute for Fluid dynamics, Chaussee de Waterloo 72, Rhode-Saint-Genese, 1640, Belgium.
E-mail address: aude.lecardonnel@vki.ac.be (A. Lecardonnel).

https://doi.org/10.1016/j.applthermaleng.2025.128034
Received 15 April 2025; Received in revised form 21 August 2025; Accepted 22 August 2025
Available online 29 August 2025

Nomenclature

Roman symbols

$\dot{m}$	Mass flow rate (kg/s)
A	Area (m^2)
Fr	Froude number
G	Mass flux $G = \frac{\dot{m}}{A}$ (kg/(s m^2))
j	Volumetric flow rate (m^3/s)
P	Pressure (Pa)
u	Superficial velocity $u = \frac{G(1-x)}{\rho}$ (m/s)
x	Vapor/gas quality $x = \frac{\dot{m}_v}{\dot{m}_v + \dot{m}_l}$ (–)

Greek symbols

χ	Martinelli parameter (–)
μ	Dynamic viscosity (Pa/s)
ρ	Density (kg/m^3)
σ	Surface tension (N/m^{-1})

Subscripts

atm	Atmospheric
a	Air
l	Liquid phase
ref	Refrigerant
sat	Saturation
s	Superficial
TP	Two-phase
tt	Turbulent–turbulent
v	Vapor/gas phase
w	Water

Abbreviations

$DIAM$	Diameter
DOE	Design of Experiment
GWP	Global Warming Potential
$HH-HC$	Horizontal Header-Horizontal Channels
$HH-VDC$	Horizontal Header-Vertical Downward Channels
$HH-VUC$	Horizontal Header-Vertical Upward Channels
$I.D.$	Internal Diameter
$INTR$	Intrusion
$OFAT$	One-factor-at-a-time
$ORIENT$	Orientation
$PANTTHER$	exPerimental And Numerical mulTiscale mulTiphasic Heat ExchangeR
POS	Position
ROI	Region of interest
SPL	Splashing grid
STD	Standard deviation
VCS	Vapor Cycle System
$VDH-HC$	Vertical Downward Header-Vertical Channels
VFM	Venturi Flow Meter
$VUH-HC$	Vertical Upward Header-Vertical Channels
WAT	Water

been dedicated to the characterization and prediction of this liquid/gas flow distribution over the last decades as it is a complex problem to address, depending on various physical phenomena but also on many parameters such as geometrical features and operating conditions. Furthermore, the flow distribution also varies with the working fluid and their phase properties. Lastly, the majority of the studies focuses on the effect of single variable for a specific flow orientation (i.e. vertical or horizontal). Thereby, the combined effect of several parameters is not thoroughly addressed in the literature [4,5]. For all these reasons, it is still rather hard to draw conclusions and obtain general design rules for the evaporator header. The present paper aims to overcome these limits, by evaluating the effect of multiple combined parameters.

Maldistribution in parallel channels of evaporators is a significant problem that arises due to the presence of valves or other components that impact the pressure drop of the refrigerant and may cause evaporation. As a result, the liquid and the vapor phases distribute unevenly in the tubes, leading to uneven cooling performance, reduced efficiency, and potential damage to the system. Flow non-uniformity among the channels is to be avoided especially for the liquid phase, as underfed channels may lead to the total vaporization of the liquid after leaving the header, and lead to dry-out which drastically decreases the heat transfer at the wall [3]. For these reasons, it is paramount to understand which parameters and their combinations might influence the distribution. This flow maldistribution has been extensively studied in the literature.

Some exhaustive reviews have already been published about the parameters influencing the distribution and whether their impact can be considered to be major or minor. Among them, the reviews of S.Y. Lee [6], Dario et al. [4] and Xiong et al. [5] are detailed and listed all the parameters that are found to influence the flow distribution, from the geometry, to the operating conditions and the fluid properties (see Fig. 1). These parameters impact the forces acting on the flow. Indeed, besides the usual forces that can be found in single fluid flows (inertial, gravitational and viscous forces), two-phase flows present surface tension forces at the liquid–vapor/gas interfaces due to the interaction between the two phases.

The reviews of Dario et al. [4] and S.Y. Lee [6] draw the same conclusion: only some of these parameters have a strong influence on the distribution and are highlighted by a red star symbol in Fig. 1, the rest of them being of minor influence. The impact of the most influencing parameters was assessed by various experimental studies. The literature review in the following Sections 1.1–1.3 is structured into three subsections respectively focusing on the geometrical parameters, the operating conditions and the fluid properties.

1.1. Geometrical parameters

The geometrical parameters are the subjects of only few studies when it comes to flow distribution. Besides, the influence of some factors such as the channels geometry and number, or the header geometry is rather nonexistent. The main factors among the geometrical parameters that present a strong impact are the channels intrusion inside the header, mostly studied by J. K. Lee and al. [7,8], but also the feeding tube hydraulic diameter and length [9,10] and finally its position on the header. However, varying the dimensions of the feeding tube is rather equivalent to varying the inlet flow patterns, and the influence of the inlet flow regimes on the distribution will be developed in the following Section 1.2. In two distinct experiments, J. K. Lee firstly studied different intrusions depths of 0, $\frac{1}{8}$, $\frac{1}{4}$ and $\frac{1}{2}$ of the square shape header width of 24 mm [7], in a vertical upward header having a feeding tube of the same dimensions as the header. The flow distributions of the air/water mixture were studied for each intrusion at mass flux of 54–134 kg/(s m^2) and inlet quality of 0.2–0.5. Secondly, J. K. Lee et al. [8] studied intrusion depth of 0, $\frac{1}{8}$ and $\frac{1}{4}$ in a 16 mm square shape header. The mass flux and inlet quality of the air/water mixture were 40–150 kg/(s m^2) and inlet quality of 0.1–0.4. Two configurations were experimented: an upward vertical header and a horizontal header with horizontal channels.

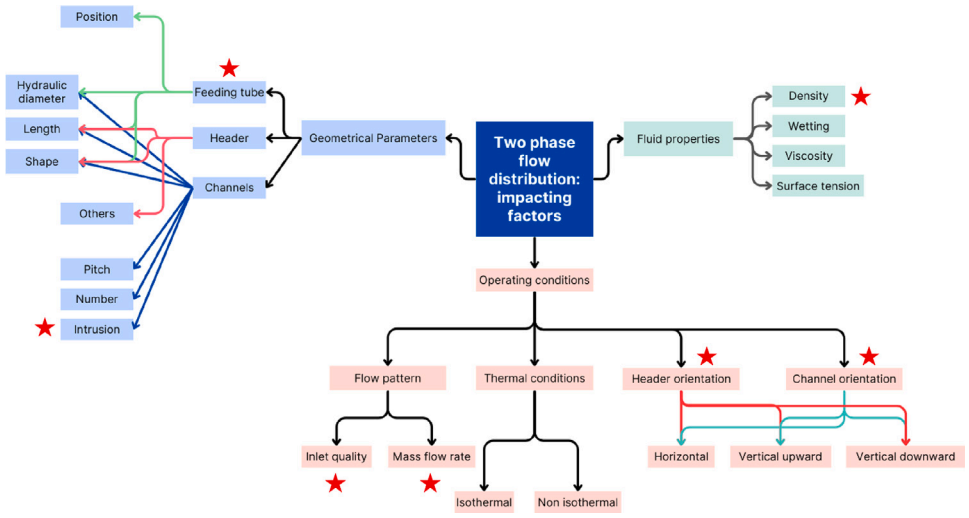

Fig. 1. Parameter impacting the two-phase flow distribution inside the header with multiple parallel channels. *Source:* adapted from Dario et al. [4].

Two conclusions could be drawn from these experiments. The first one is that the tube intrusion in a horizontal header with horizontal channels seems to worsen the distribution as it amplifies the maldistribution problem associated with this configuration. Indeed, the tube intrusion seems to decrease the liquid feeding in the first channels and to increase it in the last. In a horizontal header, since the first tubes are already underfed and the last ones overfed, the liquid maldistribution is amplified, while the vapor distribution is nearly not altered and rather homogeneous in all cases. For the upward vertical header, it is the opposite. The first channels are originally overfed in the case of no intrusion while in the last region where recirculation occurs, not enough liquid is distributed. The vapor phase exhibits the inverse trend. Thus, the tube intrusion tends to improve both the liquid and vapor distributions.

However, it appears from both studies [7,8], that in an upward vertical header, an optimal tube intrusion exists which seems to be around $\frac{1}{8}$ of the header width in both studies. When this tube intrusion is exceeded or is worth 0, the liquid and vapor distribution is worsen.

Those two studies allow an investigation of the impact of the number of channels on the flow distribution as well as the header size. Indeed, in both [7,8], the operating conditions are very similar, but the number of tubes differs from being 6 in [7] to 15 in [8], and the square shape header size from 24 mm to 16 mm. The results in term of liquid distribution show the same global trend from overfeeding of the first tube to underfeeding of the last ones. However, in the case of the 6 tubes study in [7], the tendency is very pronounced and the plateau found in the central part of the curve in the case of 15 tubes is not present at all. Thus, it means that the overall maldistribution tendency is not affected by the amount of channels, but is flattened when the number of tubes is increased, as long as liquid still reaches the last tubes.

Other relevant geometrical factors are the inlet feeding tube and the outlet tube positions. Generally, for an horizontal header, an inlet tube coaxial with the header is to be avoided as it leads to the least uniform distribution, as reported by both Cho et al. [11] and Kim et al. [12]. A position of the feeding tube perpendicular to the header or to both the header and the channels is to be preferred to improve the distribution. For a vertical header, the conclusions obtained in the literature are also congruent. Both Dario et al. [13] and Byun et al. [14] found the top inlet to enable a more homogeneous distribution of an air and water flow and a R410A flow respectively, when compared to a middle inlet position. The position of the outlet tube is fewly studied in the literature. Buyn et al. [14] however investigated its impact in the second pass of an evaporator with a vertical header. They concluded that a top or bottom outlet position enhance the distribution compared to a middle position. Finally, Kim et al. [15] examined the impact of parallel or reverse directions of coaxial inlet and outlet. These configurations are also named “Z-shape” and “U-shape”. The tests were performed in a simplified evaporator with a horizontal header connected to both vertical downward and upward channels, with air and water as fluids and quality up to 0.4. They found that the impact on the water flow distribution was negligible.

1.2. Operating conditions

The operating conditions that affect flow distribution can be categorized in three groups: flow pattern, thermal condition and header–channel orientation. For what concerns the thermal condition, it should be highlighted that most of the studies on flow distribution are achieved in adiabatic conditions, i.e. with no heat transfer nor phase change. One of the few diabatic study is performed by Vist et al. [10] using R134a in vertical upward and downward flow configurations and water as secondary fluid. The water inlet temperature was varied from 40 °C, to 50 °C and up to 60 °C in a 16 mm manifold and then in a 8 mm manifold. Apart from the case at 40 °C in the 8 mm header that exhibits a vapor distribution slightly improved, no effect at all of the water inlet temperature variation could be detected. Similar conclusions were obtained by Hwang et al. [16] who examined the influence of various heat loads (0 kW, 4.06 kW and 8.02 kW) on the two-phase distribution of a R410A flow in a horizontal header with vertical upward channels. The findings of this research indicated that the impact of mass flow rate and inlet steam quality was greater than that of thermal load. In fact, the liquid distribution variations related to the heat load were within the measurement uncertainties. Taken together, these diabatic results suggest that the onset of phase change downstream does not measurably alter the two-phase feeding of the channels in the header. Thus, the header liquid–vapor distribution can be modeled and studied as an adiabatic process.

The header and channels orientation can be combined into 5 configurations that are shown in Fig. 2. Depending on the orientation, the flow distributions present very different behaviors because of the impact of the forces acting on the fluid. A general study is given by J. K. Lee in [17] that covers all the configuration except the vertical downward header with horizontal channels. In the case of vertical upward header, vapor distribution is rather homogeneous even if the last channel receive slightly more vapor. However, concerning the liquid distribution, due to the gravity force acting in the opposite

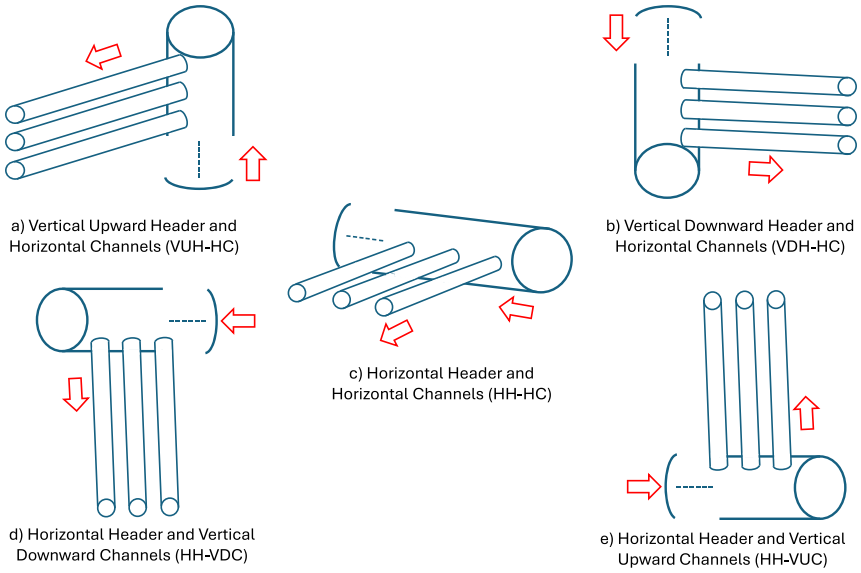

Fig. 2. All possible header and channels configurations.

direction of the flow, the first channels tend to be overfed while the last ones do not receive any liquid. As the mass-flow rate increases, this trend remains unchanged, but liquid reaches and feeds the last channels. At even higher mass-flow rates, a recirculation zone at the end plate of the header starts to appear, and the overfeeding of the last channels becomes as high as the first ones. For a vertical downward header with horizontal channels, the distribution shows a similar but opposite trend [18,19]. Indeed, in that case the gravity acts with and not against the flow, and thus pushes the liquid phase to accumulate at the bottom part of the header. Thus, the last channels present a high liquid overfeeding along with the couple of first channels, and this phenomenon is amplified as the mass-flow rate increases. The vapor phase shows a more homogeneous distribution, even if the feeding of the tubes tends to slightly but continuously increase in the axial direction of the header. As shown in [7,8], the distribution in the vertical upward header with horizontal channels can be improved by tube intrusion. However, for a vertical downward header with horizontal channels, no example of distribution improvement has been found in literature. The horizontal headers have been the most widely studied configurations. Concerning the upward flow in vertical channels, the work of Vist and Peterson [10], Hwang et al. [16] and J.K. Lee [17] observed similar liquid and vapor phase distributions. They both exhibit step-like shapes, but in an opposite trend. Indeed, the liquid phase overfeeds the last channels, which accumulates at the rear part of the header, due to the difficulty of the fluid to flow against the gravity force, while the first ones receive almost no liquid mass flow rate. For the vapor phase, it is exactly the opposite. The first channels receive almost only vapor, while the last ones, due to the liquid accumulation that creates a blockage, are highly underfed. When the channels are oriented horizontally as well as the header, the flow does not have to overcome the gravity force and thus more liquid is distributed in the first channels, even if the division remains strongly non homogeneous as reported by Jun Kyoung Lee [17]. Due to the diminution of the liquid blockage effect in the rear part of the header, more vapor is received by the last channels, allowing a quite homogeneous distribution of the vapor phase among the tubes. The last configuration concerns horizontal headers connected to vertical downward channels. As reported by Lee [17] and Kim et al. [12], the vapor phase is almost equally distributed between all the channels as it can flow in the entire header since no liquid is accumulated anywhere due to the gravity forcing the liquid to flow down in the channels. However, the situation is different for the liquid phase. Indeed, almost all the liquid flow is distributed in the first channels while from the channels located in the middle of the header until the last ones, no liquid is received. When the mass-flow rate is increased and due to the annular flow pattern, some liquid reaches the rear part of the header and thus feeds the last tubes. The distribution improvement has been widely studied by the work of Fei and Hrnjak [9], and Ahmad et al. [20,21]. Firstly, Fei and Hrnjak decreased the feeding tube length to generate a jet to allow the distribution of liquid to further down the channels. They also noticed that by generating a mist flow pattern inside the feeding tube, a good liquid distribution could be obtained. Ahmad used a splashing grid at the end of the feeding tube to create droplet jets, reproducing the effect created by a mist flow pattern. Thanks to this device, good vapor and liquid distributions could be obtained. Other devices and solutions exist or are under study to help the uniformity but will not be developed in the present article. One may read the above mentioned reviews of Dario et al. [4] and Xiong et al. [5] for further information.

1.3. Fluid properties

The flow maldistribution in headers in the literature is generally analyzed for one specific fluid. Thus, this raises the question of the validity of this improvement when using other fluids. This subject has been dealt with only few studies, but their conclusions are however consistent. Zhang et al. [22] tested both R134a and water/air mixture under similar conditions, and they observed different flow distributions between the two fluids. They explained these results by the difference in fluid properties. Indeed, R134a and air/water mixture present different liquid to vapor phase density and viscosity ratios $\frac{\rho_l}{\rho_v}$ and $\frac{\mu_l}{\mu_v}$. This directly impacts the predominance of the forces acting of the flow, and thus the flow patterns. Indeed, for the same mass flux G and quality x [22], R134a present mostly stratified structures, while air/water mainly exhibits annular flow regimes. Thereby, depending on the flow pattern in the feeding tube, the distribution in the same header will be strongly influenced. This is confirmed by the studies of Kim et al. [12] and Zou et al. [23]. In Kim et al. [12] experiments obtained for R134a and air/water mixture at the same mass flux G and inlet quality x were compared, and while the vapor phase distribution is quite homogeneous in both cases, the liquid distribution is very different, as well as the inlet flow patterns. In Zou et al. [23], very different distributions were observed testing R245fa, R134a, R410a and R32 under the same operating conditions and facility. It appears also in that case that the distribution varies significantly.

1.4. Motivation of the study and objectives

Despite the literature on maldistribution is vast, the existing studies focus only on few parameter effects and the literature remains fragmented: no work to date comprehensively examines how multiple parameters collectively govern liquid maldistribution in evaporator headers. However, it is essential to investigate multiple parameters simultaneously and their mutual interactions. As a consequence, it is hard to draw general conclusions and trends about the two-phase flow distribution in an evaporator when more than two parameters are combined. There is the great need of a more complete and systematic study of the influence on the liquid distribution of the main impacting parameters. Thus, the present work aims at filling this gap in the literature. Firstly, the parameters whose interactions are of great interest were defined. A test section design was built accordingly and is described in Section 2 as long as the list of parameters. Secondly, to help building an optimized test matrix, a Design of Experiment algorithm was used. This approach is explained in Section 2.3. Then, the experimental loop is presented in Section 3, followed by the measurement methodology, the data reduction and the measurement uncertainties in Section 4. Finally, the main results of this experimental campaign are presented in Section 5. This is the first systematic study, to the authors' knowledge, investigating the impact of various combined parameters on two-phase distributions in evaporators' headers. Additionally, applying DOE methods to two-phase distributions in flow pattern similarity with refrigerant is a novelty in the field. The results of this work will show the effect of studying multiple combined parameters and will detail which combination of geometrical parameters is able to provide a uniform distribution. This approach not only represents the first application of DOE to two-phase distribution in vapor–liquid refrigerant flows, but also offers direct guidance for designing more energy-efficient evaporators with uniformly split flows — an outcome with clear implications for next-generation refrigeration and heat-pump technologies.

2. Test section design

2.1. Operating conditions

As outlined by the literature review, the use of different fluids for the same set-up and operating conditions leads to different distribution results. The current framework of this study is to obtain some deeper understanding about the two-phase flow maldistribution in a simplified evaporator header working with an air/water mixture. The conclusions provided by this study are meant to be extended and used to design evaporators working with refrigerants. Thus, there is the need to carry a flow pattern similarity study between the air/water mixture and the R1234ze(E), which is the low Global Warming Potential fluid selected for this two-phase flow pattern similarity.

In Webb et al. [24], a flow pattern similarity between the R-404A refrigerant and an air–water mixture was achieved by keeping three non-dimensional numbers constant, assuming that the geometrical features of the facility are equal. The first one to be kept constant between the two cases is the phase density ratio $\frac{\rho_l}{\rho_v}$, as Zhang et al. [22] also showed the great importance. The fluid properties of R1234ze(E) (liquid and vapor phase viscosity and density) are displayed in Table 1 at T_{sat} = 0 °C). Given the air properties, to reach such a goal, the air needs to be operated at 8 bar absolute pressure to obtain the targeted density. Due to material constraints, the maximum operating pressure was limited to 7 bar, which did not allow for an exact density ratio similarity (see Table 2).

The surface tension σ_l is also a significant element to consider. Indeed, the surface tension value of water in contact with air at atmospheric pressure and 20 °C is 73 mN m^{-1} and decreases only very slightly with pressure [26]. Since the surface tension value that can be commonly found for refrigerant is ~10 mN m^{-1}, the variation is expected to affect the conclusions as well in term of distribution. However, the surface tension is especially significant when it comes to micro-channels. Commonly, the header and feeding pipes dimensions of evaporators are not of the order of micro-millimeter but at least around ten times higher. Thus, the phase density ratio $\frac{\rho_l}{\rho_v}$ similarity is considered to be significantly more impacting than the surface tension value similarity.

Table 1
R1234ze properties at T_{sat} = 0 °C [25].

μ_l Pa/s	μ_v Pa/s	ρ_l kg/m^3	ρ_v kg/m^3
$2.69 \cdot 10^{-4}$	$1.12 \cdot 10^{-5}$	1240.6	11.65

Table 2
Similarity study.

Parameter	Refrigerant		Air/water	
x	0.04	0.4	0.042	0.41
Min $\dot{m}_v$ (g/s)	4	40	**3**	30
Min $\dot{m}_l$ (g/s)	96	60	69	**43**
Max $\dot{m}_v$ (g/s)	10	100	7.6	**76**
Max $\dot{m}_l$ (g/s)	240	150	**173**	108
$\frac{\rho_l}{\rho_v}$	106	106	120	120

The second parameter defined by Webb [24] is the Martinelli parameter χ_{tt} which is a sort of liquid fraction in case of both phases in turbulent regime and is defined as

$$\chi_{tt} = \left(\frac{\rho_v}{\rho_l}\right)^{0.5} \left(\frac{\mu_l}{\mu_v}\right)^{0.125} \left(\frac{1-x}{x}\right)^{0.875}. \quad (1)$$

Finally, the third parameter is the densimetric Froude number F_{TD} that compares the inertial and the gravity forces acting on the fluid. It is expressed as

$$F_{TD} = \left(\frac{\rho_v j_v^2}{(\rho_l - \rho_v) D \cdot g}\right)^{0.5}, \quad (2)$$

where j_v is the vapor volumetric flow rate. This formulation accounts for the impact of the lighter phase on the buoyancy force by including the reduced gravity under Boussinesq approximation, valid in the present work. The purpose of fixing the Martinelli and densimetric Froude between the R1234ze(E) and the air/water mixture is to ensure that equivalent flow patterns would be studied, since flow regimes in the feeding tube influence strongly the distribution of the two phases [9]. Based on these three parameters, on the required operating conditions (100 g/s < $\dot{m}_{refrigerant}$ < 250 g/s and 0.04 < $x_{refrigerant}$ < 0.4) and on the properties of the fluids (air, water and R1234ze(E)), the results of the flow pattern similarity study are presented in Table 2. In a first time, the density ratio, the Martinelli parameter χ_{tt} and the densimetric Froude number F_{TD} are calculated for the R1234ze(E) operating conditions. In a second time, the required equivalent qualities of the air/water mixture is obtained from the Martinelli parameter and density ratio similarities. Then, the required air mass flow rates are calculated from the densimetric Froude number similarity and more specifically through the vapor phase volumetric flow rate j_v. Lastly, the water mass flow rates are retrieved from both the quality and the air mass flow rate.

Thereby, air mass flow rates ranging from 3 g/s to 76 g/s are required along with water mass flow rates ranging from 43 g/s to 173 g/s (indicated in bold font in Table 2), with the equivalent targeted quality values x from 0 to 0.41. Based on the equipment capabilities, it was decided to test 6 inlet flow rate conditions: water mass flow rates $\dot{m}_{water,inlet}$ of 100 and 160 g/s, combined to qualities of 0.04, 0.1 and 0.25. These values correspond to air mass flow rates $\dot{m}_{air,inlet}$ ranging from 4.2 g/s to 53.3 g/s.

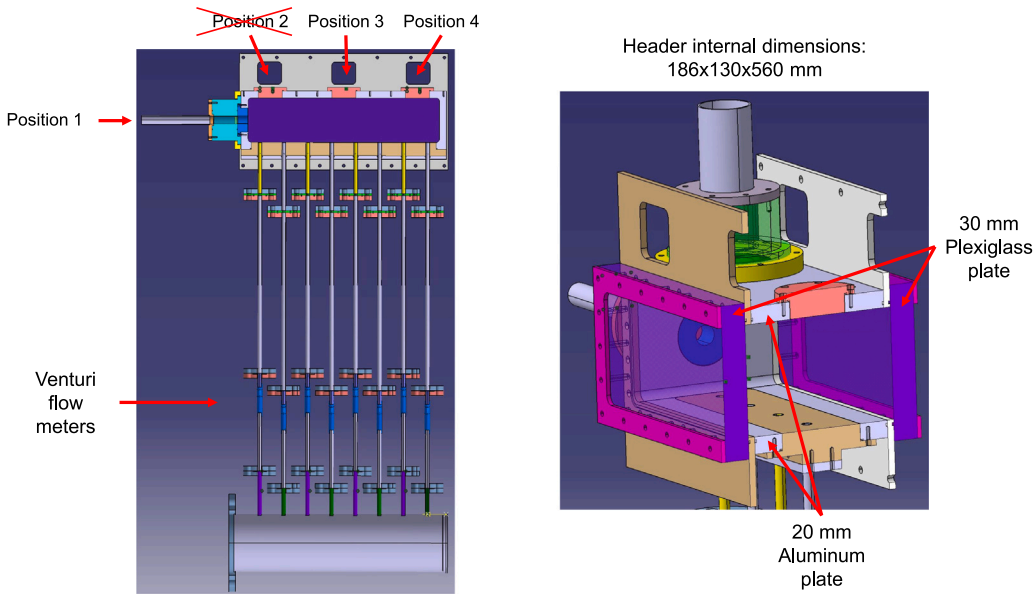

Fig. 3. Test section design: (Left) Front view, (Right) Close view of the header.

2.2. Geometrical dimensions

The calculation of the geometrical dimensions and the design of the test section were based on three characteristics:

1. The most impacting parameters gathered from the literature review (see Section 1)
2. The traditional simplified evaporator designs found in the literature [9,20,27]
3. The similarity study (see Section 2.1)

Firstly, it appears from the literature review that the most impacting parameters among the geometrical factors (see Fig. 1) are the feeding tube position and hydraulic diameter since they impact greatly the flow pattern at the inlet of the header and thus the distribution, as well as the channels intrusion inside the header. Among the operating conditions, the channels and header orientations are found to highly influence the two-phase flow distribution as well as the flow pattern. Between the fluid properties, the density ratio between the two phases shows a substantial effect. The present test section was therefore designed to allow the study of the combined impact of the feeding tube position and diameter, the channels intrusion, the header orientation, and the density ratio between the two phases. Based on the common header and channel arrangements found in the literature, as well as the minimum and maximum mass flow rates obtained from the flow pattern similarity (Table 2), the sizing of the various components such as the feeding tube, the header, the channels and the outlet reservoir was adapted. The test section generated is displayed in Fig. 3:

It consists of a manifold made of aluminum, with a rectangular section of (186 × 130) mm, 560 mm long. The wall thickness is 20 mm to ensure a proper resistance to the 7 bar pressure. The front and back faces of the header are made transparent to enable flow visualization inside the header. The two Plexiglass windows are 30 mm thick, calculated also to guarantee a proper resistance to pressure. The metallic frames enclosing the Plexiglass were extended on the upper side to minimize the displacement of the test section when pressurized. The inlet pipe is 1 m long. It is made of stainless steel, except for 65 mm before the manifold, where it is transparent to allow the visualization of the flow regime at the inlet section of the header. The visualization piece can be observed in Fig. 4 left. It is not possible to cover all flow patterns, from stratified to annular with only one inlet pipe diameter. Thus, two feeding tube diameters were considered: 23 mm and 56 mm. The objective of the 56 mm pipe diameter is to cover all the stratified inlet flow regimes, while the objective of the 23 mm pipe is to potentially cover the remaining flow patterns: slug, intermittent, and annular. Based on the inlet air and water mass-flow rates ($\dot{m}_{\text{air,inlet}}$ and $\dot{m}_{\text{water,inlet}}$) selected that comply with the similarity study presented in Section 2.1 and the two feeding tube diameters considered, the range of total mass flux can be evaluated using

$$G = \frac{\dot{m}_{\text{air}} + \dot{m}_{\text{water}}}{A_{\text{pipe}}}, \tag{3}$$

where A_{pipe} is the cross-sectional area of the inlet feeding pipe. G then ranges from 42 kg/(s m^2) to 513 kg/(s m^2). The liquid superficial velocities u_{sl} spans from 0.04 m/s to 0.39 m/s while vapor superficial velocities u_{sv} from 0.21 m/s to 16 m/s were reached.

Four inlet pipe positions can be tested. Position 1 is referred to be coaxial to the header length, while position 2, 3, and 4 are perpendicular to the header length. For each position, the inlet pipe diameter can either be 23 mm or 56 mm. Position 2 and 4 of the feeding tube are expected to lead to similar distributions. For this reason as well as time limitations, the position 2 was not considered and its symmetrical position 4 was exploited instead. Therefore, three inlet pipe positions were in fact utilized. Eight tubes of 10 mm diameter made in stainless steel are connected to the manifold. Venturi Flow Meters (VFM) are installed in each channel to obtain the individual mass flow rates of each phase, as well as pressure sensors to monitor the static absolute pressure. An upstream length of 520 mm is available before the venturi, and a downstream length of 170 mm to respect the standard ISO 5167-4:2003 [28]. The static pressure sensor is positioned at 70 mm from the top of the tube. More details about the venturi design and calibration can be found in Lecardonnel et al. [29]. To change the channels intrusion inside the header, spacers made of stainless steel were manufactured and inserted between the pair of flanges located before the VFM. This flexible element allows to study easily several intrusion depths. Two dimensions were chosen, to enable an intrusion of the channels inside the header of $\frac{1}{4}$ and $\frac{1}{2}$ of the header height of 130 mm. The $\frac{1}{2}$ spacer can be observed in Fig. 4 (Right).

In addition, it is possible to insert a removable device called “splashing grid” (Fig. 5) between the end of the feeding tube and the inlet of the header. This system was identified as one effective way to improve flow maldistribution according to the work of Ahmad et al. [20] since it enables the breaking of the inlet flow pattern and the possible

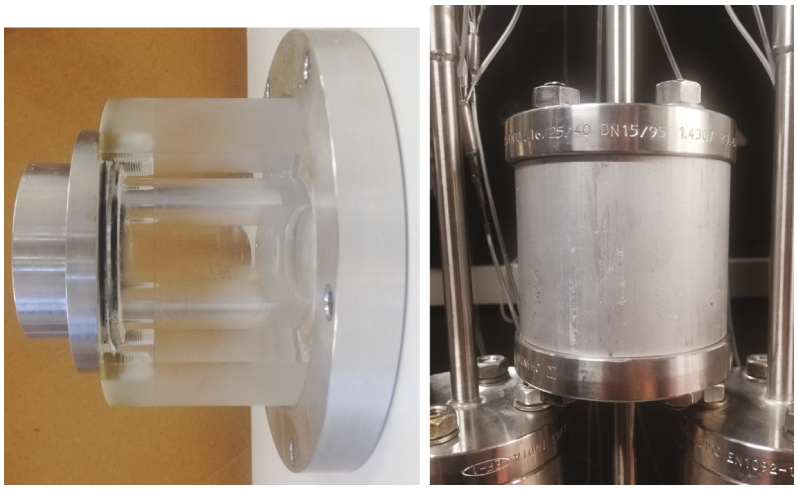

Fig. 4. (Left) Inlet transparent piece, (Right) Spacer for channel intrusions.

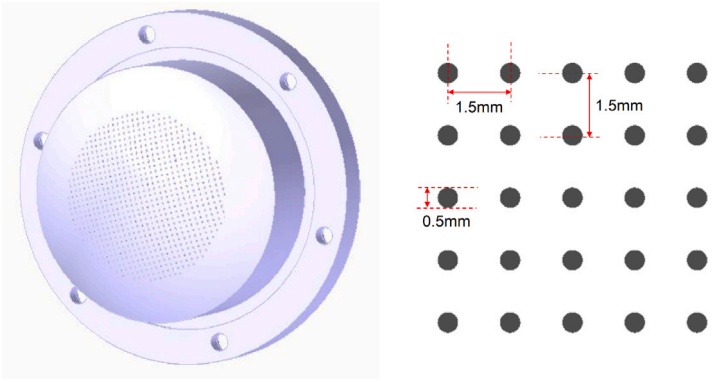

Fig. 5. (Left) Splashing grid design, (Right) Holes pattern.

phase separation. The grid was designed with similar dimensions. Holes of 0.5 mm and spaced of 1.5 mm in each direction were uniformly distributed in a squared pattern (Fig. 5). The grid was 3D printed in resin, and the wall thickness was adapted to withstand the 7 bar pressure.

Finally, the flow passing through the 8 tubes exits into a 200 mm circular collector. The outlet pipe of the test section is located on the same side as the coaxial inlet pipe position, in a "U" shape. The whole test section was screwed to a wooden plate mounted on sliding rails. This allows for a great flexibility of the structure which was a requirement since four header and channel positions out of the five displayed in Fig. 2 aimed at being investigated: configurations (a), (b), (d) and (e).

2.3. Test matrix

As highlighted by the literature review, the majority of the studies focuses on the influence of one variable or two, for instance J. K. Lee [8] analyzed the effect of the channel intrusion for two header and channel orientations. They follow the one-factor-at-a-time (OFAT) methodology: they modify each parameter over its full range, while the other parameters remain unchanged. This strategy presents however some strong limitations since the interactions between the variables cannot be examined [30], and thus the optimal combination of variables can hardly be captured. In such context of multi-factorial analysis, the use of Design of Experiments (DoE) techniques is excessively meaningful to select an optimal test matrix. Indeed, these techniques can help to build a matrix that will allow to retrieve knowledge about the influence of a single variable or of combination of variables as exactly as possible in a minimum amount of experimental tests. More information about such technique can be found in the work of Tempesti et al. [31], where the authors show a methodology based on DOE approach applied to a similar case study. The selection of the factors and levels that define the design space was explained in Section 2.2 and they are listed in Table 3. For each factor, each level was given a label and numbering between −1 and 1 included. This labeling and numbering will be referred to in the rest of the article. For instance, *Position -1* refers to the central inlet and perpendicular to the header length. Two levels of water flow rate were chosen among the possible range presented in Section 2.1. Three levels of air flow rate were as well selected to reach the various flow patterns described in Section 2.2 and are shown in Table 3 as air quality levels.

From this list, if all the combinations between factors and levels were to be tested, then 1296 experiments would be needed. With the help of a DOE algorithm, the amount of tests can be tremendously reduced while maintaining a high degree of precision in the influence of individual and combined parameters within the design space. In that context, the experimental matrix was created by means of the Python package DoEgen [32], the operation of which is briefly described herein. Once the user has defined the factors and levels of interest, the algorithm creates various experimental matrices with sequentially increasing number of tests. For each matrix, it monitors several parameters to help the experimentalist select the appropriate number of runs for the specific case under investigation. Reducing the number of tests means that not all combinations of factors and levels will be included in the experiment. To ensure that the resulting analysis remains statistically valid and consistent, the reduction must be done in a controlled way. In particular, certain statistical properties should

Table 3
Factors, numbers and descriptions of levels for each orientation.

Factor	Levels	
Header/Channels orientation	4	Orient −1: Horizontal Header and Vertical Downward Channels (HH-VDC) Orient $-\frac{1}{3}$: Horizontal Header and Vertical Upward Channels (HH-VUC) Orient $\frac{1}{3}$: Vertical Upward Header and Horizontal Channels (VUH-HC) Orient 1: Vertical Downward Header and Horizontal Channels (VDH-HC)
Inlet tube position	3	Pos −1: Perpendicular to header length, central Pos 0: Perpendicular to header length, lateral Pos 1: Parallel/Coaxial to header length
Inlet tube diameter	3	Diam −1: 23 mm Diam 1: 56 mm
Splashing grid	2	Grid −1: grid not present Grid 1: grid present
Channels intrusion	3	Intr −1: 0 mm Intr 0: 33 mm ($\frac{1}{4}$ header height) Intr 1: 66 mm ($\frac{1}{2}$ header height)
Water inlet flow rate $\dot{m}_{\text{water,inlet}}$	2	Water −1: 0.1 kg/s Water 1: 0.16 kg/s
Air inlet quality x	3	Air −1: $x = 4\%$ Air 0: $x = 10\%$ Air 1: $x = 25\%$

be preserved: for instance, each level of a factor and each combination of levels across factors should appear an equal number of times or as evenly as possible. The DoEgen package addresses this by computing a set of metrics that quantify how well these properties are maintained in the reduced experimental matrix. These cited parameters serve to evaluate how well the matrix is balanced between factors (Center balance), between levels (Level balance), between levels in pairs of factors (Two-level Balance), between factors-levels pairs combination (Two-level missing). In addition, it quantifies how much each matrix is close to an orthogonal one (Orthogonality), and it computes the D1-Efficiency, which evaluates the goodness of the experimental design according to the D-Optimal criteria. Additional information can be found in the work of Tempesti et al. [31].

The overall evolution of these efficiencies with increasing number of runs are shown in Fig. 6(Left) for the case under investigation. A zoom of the region of interest (ROI) is shown in Fig. 6(Right). At low number of runs, all efficiency metrics are understandably low – this is expected, as there are not enough tests to ensure balance across the design space. As the number of runs increases, the efficiency values rise steadily, reaching a first local maximum at 24 runs, where both center and level balance reach 100%. This indicates that each factor and level appears an equal amount of times. Notably, the total number of combination divided by 24 is an integer, which allows perfect distribution. However, beyond this point, adding more runs does not necessarily improve the design quality. In fact, the metrics may decrease temporarily because some factors or levels start appearing more frequently than others, disrupting the balance. As the number of tests continues to increase, a second optimal point is reached at 48 runs, where center and level balance return to 100%, and two-level balance improves compared to the 24 run case. Thereby, this test matrix of 48 sets of header/channel orientation, inlet tube position and diameter, presence/absence of the splashing grid, channel intrusion, one specific combination of water and air flow rate levels generated by the algorithm was selected. It should be noted that this matrix selected 12 experiments per header and channels orientation. In addition, besides the specific combination of water and air flow rates levels selected by the algorithm, the other 5 combinations of water and air levels were as well tested for each of the 48 configurations. Indeed, it did not require a tremendous additional amount of time but the additional information gathered was of great significance as it allowed to draw conclusions about the stability of the two-phase distribution over various air and water conditions.

2.4. Flow maps

As stated in Sections 1.2 and 2.2, the flow pattern inside the feeding tube is of great interest as it will drive the behavior of the two-phase flow inside the header and the distribution among the channels. The characterization of such flow patterns depends not only on the fluid employed, but also on the pipe diameter and orientation. In the following paragraphs, the flow pattern predictions are presented per feeding tube orientation.

2.4.1. Horizontal pipe

For a horizontal pipe, the Baker flow map [33] is very often reported in the literature [34–36] to translate accurately the transitions of the flow regimes from one fluid to another one. The Baker flow map (see Fig. 7) is built with air and water at atmospheric pressure and ambient temperature as reference and the transitions between the flow pattern are quantified in terms of air mass flux $G_{\text{a,B}}$ and water mass flux $G_{\text{w,B}}$ where B refers to Baker. Two parameters λ and Ψ (Eqs. (4) and (5)) are defined by Baker to relate the vapor and liquid properties of any fluid considered to the properties of air and water at atmospheric pressure and ambient temperature. They are evaluated using

$$\lambda = \left(\frac{\rho_{\text{v}}}{\rho_{\text{a}}}\frac{\rho_{\text{l}}}{\rho_{\text{w}}}\right)^{1/2} \tag{4}$$

and

$$\Psi = \left(\frac{\sigma_{\text{w}}}{\sigma}\right)\left[\left(\frac{\mu_{\text{l}}}{\mu_{\text{w}}}\right)\left(\frac{\rho_{\text{w}}}{\rho_{\text{l}}}\right)^{2}\right]^{1/3}. \tag{5}$$

The air and water mass fluxes $G_{\text{a,B}}$ and $G_{\text{w,B}}$ and the parameters λ and Ψ are related to the vapor and liquid mass fluxes of any fluid G_{v} and G_{l} using

$$G_{\text{w,B}} = G_{\text{l}}\Psi \tag{6}$$

and

$$G_{\text{a,B}} = \frac{G_{\text{v}}}{\lambda}. \tag{7}$$

Then, the flow pattern transitions in term of mass flux of any fluid are calculated with

$$G_{\text{l}} = \frac{G_{\text{w,B}}}{\Psi} \tag{8}$$

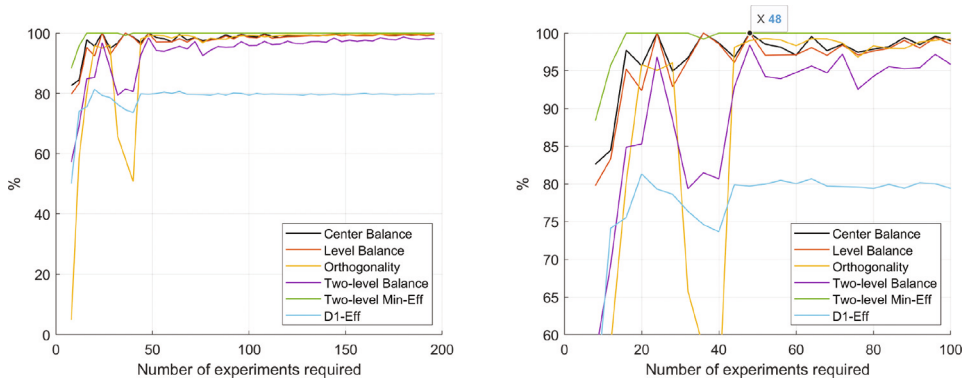

Fig. 6. (Left) Overall evolution of efficiencies in percentage with number of experiments required, (Right) Zoom in the ROI.

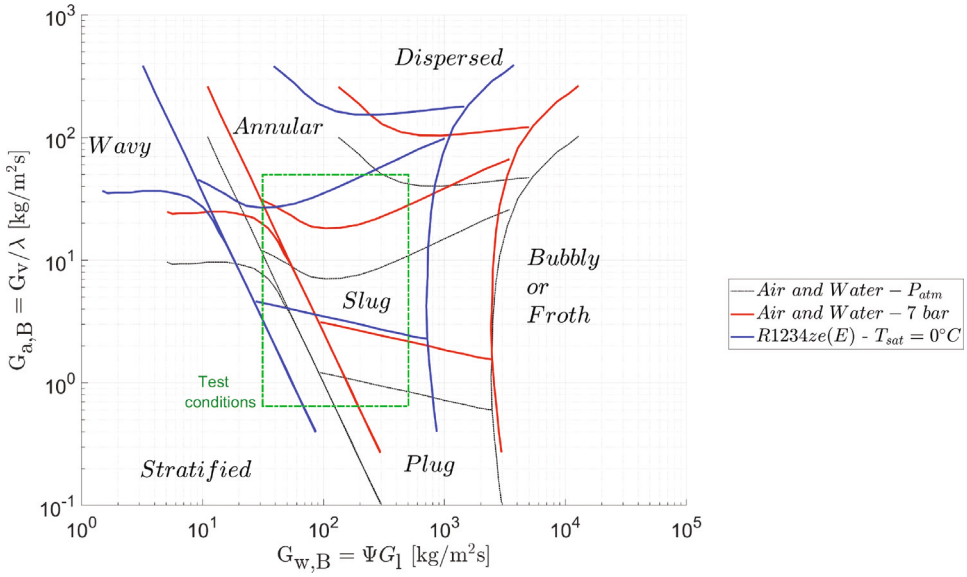

Fig. 7. The basic Baker flow map compared to transitions for air and water at 7 bar and R1234ze(E) at $T_{sat} = 0$ °C.

and

$$G_v = G_{a,B}\lambda. \tag{9}$$

The transitions lines between the various flow patterns were calculated for air and water at 7 bar, pressure imposed by the similarity study (see Section 2), and are compared to the actual transitions of the Baker flow map based on air and water at atmospheric pressure and ambient temperature in Fig. 7. The transitions of a typical low Global Warming Potential (GWP) refrigerant (R1234ze(E)) are as well displayed for a sake of comparison. They are calculated at a saturated temperature $T_{sat} = 0$ °C which is a common operating temperature in an evaporator exploiting a GWP refrigerant.

Overall, as one can notice, the flow regimes transitions of air and water at 7 bar occurs at higher vapor mass fluxes, and at both higher liquid and vapor mass fluxes for the stratified and wavy transitions when compared to the original transitions of the Baker flow map. Concerning the R1234ze(E), the flow transitions occurs at higher vapor and lower liquid mass fluxes. Due to the density ratio similarity, the flow transitions between the annular, slug and plug flow patterns occur at very similar vapor mass fluxes between the air and water at flow at 7 bar and the R1234ze(E) flow at $T_{sat} = 0$ °C. in Fig. 7, the window of the test conditions targeted which were presented in Sections 2.1 and 2.2 is displayed. This covers as expected the following flow regimes: stratified, plug, slug and annular.

2.4.2. Vertical upward pipe

For a vertical upward pipe, the Hewitt and Roberts flow map [37] is trusted to be able to predict the transitions of a wide range of fluid [38] and is displayed in Fig. 8. This flow map relates the flow patterns transitions to both the vapor and liquid momentum fluxes $\frac{G_v^2}{\rho_v}$ and $\frac{G_l^2}{\rho_l}$.

To compare the evolution of the flow regime conditions between the air/water and the R1234ze(E) flows, the same inlet vapor and liquid mass fluxes G_v and G_l (corresponding to the superficial velocities mentioned in Section 2.2) were considered for the calculation. The superficial momentum fluxes $\frac{G_v^2}{\rho_v}$ and $\frac{G_l^2}{\rho_l}$ were then calculated based on the densities corresponding to the air/water mixture at both atmospheric pressure and 7 bar and room temperature and to the R1234ze(E) at $T_{sat} = 0$ °C. The test points are again shown in the shape of a window for a sake of clarity in Fig. 8. As one can conclude from the figure, the annular flow regime is more difficult to reach for air and water at 7 bar as well as for R1234ze(E) at $T_{sat} = 0$ °C. Indeed, to reach it it requires vapor momentum fluxes respectively ~7 to ~12 times higher than for air and water at atmospheric pressure. This is

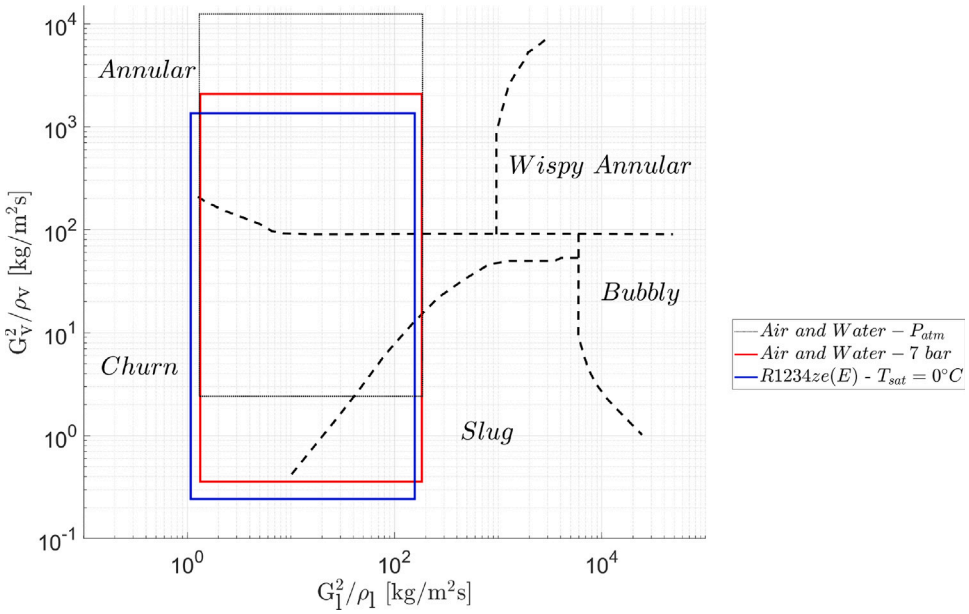

Fig. 8. The basic Hewitt flow map comparing the flow regime evolutions for air and water at 1 bar, at 7 bar and for R1234ze(E) at T_{sat} = 0 °C.

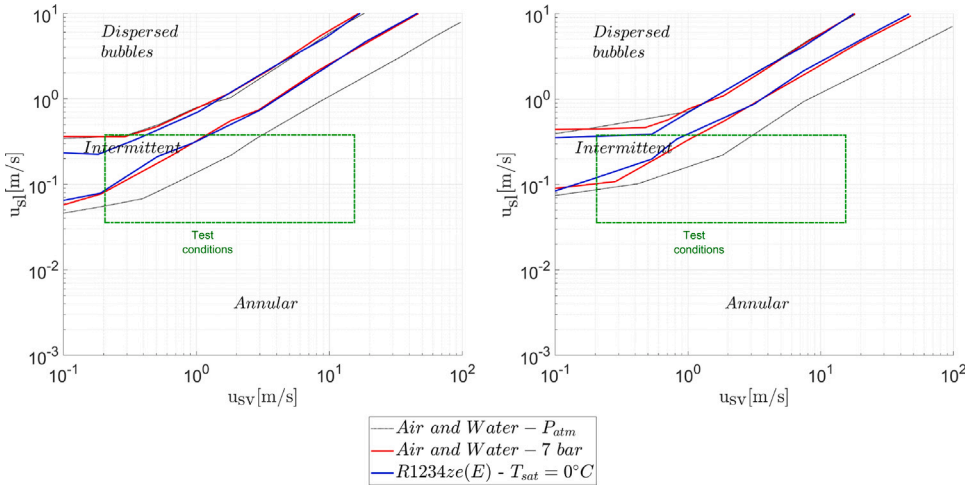

Fig. 9. Flow pattern transition comparison in a vertical downward pipe for air and water at 1 bar and at 7 bar and for R1234ze(E) at T_{sat} = 0 °C in a feeding tube of: (Left) 23 mm diameter, (Right) 56 mm diameter.

equivalent to the density ratio between air at 7 bar and the vapor phase of R1234ze(E) with the air at atmospheric conditions. The flow regimes covered in the present study are as targeted slug, churn and annular.

2.4.3. Vertical downward pipe

For a vertical downward pipe orientation, no generalized flow map could be found. However, Barnea developed a unified flow scheme that allows for the prediction of flow maps for all pipe inclinations, but also for all pipe diameters and fluids [39]. This scheme was implemented, and the flow pattern transitions for a vertical downward pipe obtained for an air/water mixture at 1 bar and at 7 bar, and for a R1234ze(E) flow at a saturation temperature T_{sat} = 0 °C are compared in Fig. 9. The flow pattern transitions are function of the superficial velocities of the two phases u_{sl} and u_{sv}. In Fig. 9 (Left), the flow pattern comparison is achieved for the 23 mm diameter feeding tube, while Fig. 9 (Right) depicts the comparison for the 56 mm diameter feeding tube.

As can be noticed, only three flow patterns are encountered in vertical downward pipes: dispersed bubbles, intermittent and annular. The test conditions did not however allow the dispersed bubbles flow regime to be reached. The two flow pattern transitions (DB–I and I–A) are logically expected to occur at lower liquid superficial velocities u_{sl} in the 23 mm diameter pipe than in the 56 mm diameter. Besides, as one can note from Fig. 9, the flow pattern transitions greatly match between the air/water mixture at 7 bar and the R1234ze(E) at T_{sat} = 0 °C, apart for a small region of the DB–I transition for the 23 mm diameter tube and at low u_{sv}. However, while the DB–I flow transition is found to be very similar for the air/water at 1 bar and the other two flows, the I–A transition differs. Indeed, annular flow patterns can be reached at lower liquid superficial velocities u_{sl} but higher vapor superficial velocities u_{sv} for the air/water at 1 bar. In this downward orientation, the gravity acts with the flow. Thereby the higher is the density, the higher is the inertial force magnitude. This explains why the flow transition to annular occurs at lower u_{sl} for the air/water mixture at 7 bar and the R1234ze(E) at T_{sat} = 0 °C than for the air/water at 1 bar.

2.4.4. Conclusion

To conclude on the study of all these flow maps, the main important finding is that the existing studies about maldistribution that use air

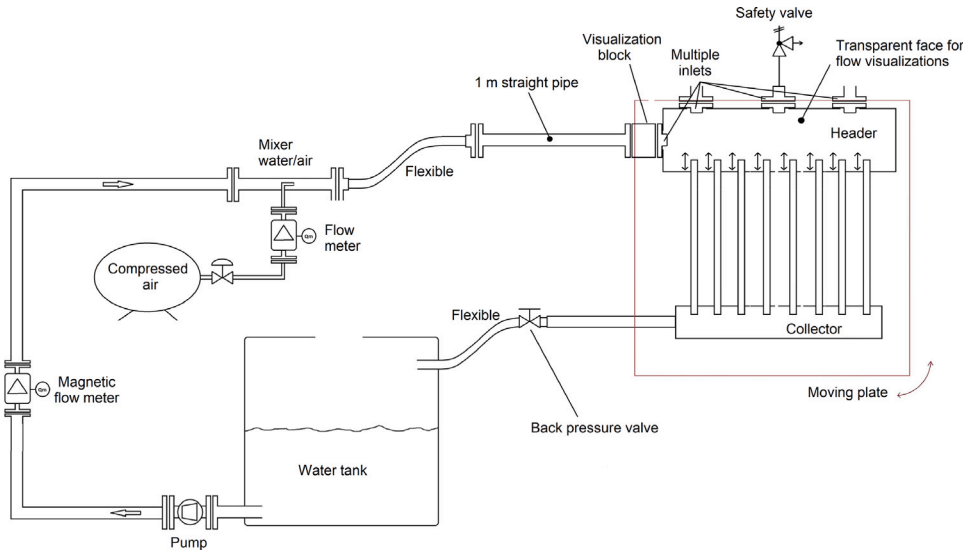

Fig. 10. Experimental apparatus of the adiabatic set-up.

and water at atmospheric pressure are very likely not representative of the actual flow pattern conditions inside an evaporator. Indeed, due to the difference of liquid and especially vapor phases between air/water at P_{atm} and a refrigerant, the magnitude of the various forces acting on the fluid is greatly altered, and thus this leads to a significant shift in the flow regime transitions.

3. Experimental loop

The overall experimental apparatus is shown on Fig. 10. An air/water mixture is used as a fluid. Water is pumped from a tank by a centrifugal pump (Wilo Helix V 214-1/16/E/KS/400-50) and its flow rate is measured thanks to an electromagnetic flowmeter (Fuji Electric ModMAG® M1000). A 15 bar compressed air line is connected to the facility and its pressure is then decreased to around 7.5 bar through a pressure regulator. The air flow rate is measured by means of a thermal mass flow sensor (CS Instruments VA 500). Air and water are then mixed together by means of an elbow pipe inserted in the main water pipe. The mixture is then further sent to a straight length of pipe to ensure a fully developed flow at the inlet of the test section. The test section is connected to the rest of the facility by means of flexible hoses. Since four header and channel orientations were to be tested, there was the need to have easily adjustable connections. A safety bar with USV 112-12, DN40 with adjustable pressure range 2–12 bar, set to 8 bar maximum pressure and a maximum exit flow rate of 13.1 m^3/h is connected to one of the inlet ports of the test section. Downstream the test section, a back pressure valve allows for the pressurization of the test section to the desired pressure condition. Finally the air and water mixture is sent back to the water tank. The water is collected at the bottom while the air is released to the surroundings.

4. Data reduction, uncertainties and comparative response variable

All the instruments described in the preceding paragraphs were connected to a NI-DAQ (National Instruments) hardware for signal acquisition. This includes the water electromagnetic flow meter for $\dot{m}_{water,inlet}$, the air thermal flow meter for $\dot{m}_{air,inlet}$ and the pressure membrane sensor for $\Delta P_{venturi,TP}$. All signals were recorded at a frequency of 200 Hz over a duration of 90 s.

The inlet quality x was determined using Eq. (10)

$$x = \frac{\dot{m}_{air,inlet}}{\dot{m}_{air,inlet} + \dot{m}_{water,inlet}}. \tag{10}$$

Table 4
Uncertainty estimation.

Variable	Evaluation	Uncertainty value
Inlet water flow rate $\dot{m}_{water,inlet}$	Manufacturer	0.3%
Inlet air flow rate $\dot{m}_{air,inlet}$	Manufacturer	1.5%
Venturi pressure drops $\Delta P_{venturi,TP}$	Manufacturer	154 Pa
Inlet quality x	Calculated (Eq. (10))	[0.00059–0.0029]

The individual air and water flow rates for each of the eight channels, denoted as $\dot{m}_{water,channel,i}$ and $\dot{m}_{air,channel,i}$ respectively (where i represents the channel number from 1 to 8), were derived from the venturi pressure drop $\Delta P_{venturi,TP}$ measurements and a robust calibration dataset obtained prior to the experimental campaign. For a detailed explanation of the calculation methodology, readers are referred to the article by Lecardonnel et al. [29]. The accuracy of the individual air flow rate measurements is estimated to be within ±20% on average, while the accuracy for the water flow rate measurements is expected to be within ±10% on average.

The uncertainty values estimated for parameters of interest, measured or calculated, are listed in Table 4.

To compare the measurement results and determine whether a specific parameter or level improves or worsens the distribution among the channels, a comparative response variable must be defined. In an evaporator, liquid phase distribution is more crucial than vapor phase distribution to avoid dry-out phenomena. As a consequence of this observation, as the comparative response variable for post-processing, the standard deviation of the water flow distribution among the eight channels was selected. The standard deviation indicates how far the actual distribution deviates from the ideal uniform distribution among the eight channels. It is calculated using

$$STD_{water} = \sqrt{\frac{1}{n-1}\sum_{i=1}^{n} |\dot{m}_{water,channel,i} - \dot{m}_{\mu}|^2}, \tag{11}$$

where n is equal to 8 as the total number of channels. The water flow rate mean value $\dot{m}_{\mu}$ across the eight channels is defined as

$$\dot{m}_{\mu} = \frac{1}{n}\sum_{i=1}^{n} \dot{m}_{water,channel,i} = \frac{\dot{m}_{water,inlet}}{n}. \tag{12}$$

5. Results

A schematic of each orientation can be found in Fig. 2 along with the abbreviations for the header/channel orientations used in the results

discussion. Firstly, the overall results of the study are presented through a DOE mean plot that allows to know the ranking of the most affecting parameters. The combination of parameters leading to the best and the worst expected distributions is given, and the water distribution profile from the tests with the closest combinations are presented. Secondly, the experimental results obtained in the present work are compared with other relevant works in the literature. Thirdly, the combined effect of the feeding tube position and diameter, as well as the channels intrusion and the presence/absence of the splashing grid is analyzed for each of the header and channels orientation. Finally, a summary of the main conclusions are gathered for each orientation and an attempt of design rules are produced.

5.1. Overall results

5.1.1. Ranking of most impacting parameters

A ranked order listing of the most affecting factors can be obtained with the so-called "DOE Mean plot" shown in Fig. 11. It indicates the average comparative response variable y (i.e. STD_{water}) in the y-axis for each level of the factors in the x-axis. The response variable results for each level of each factor are represented by a black X. The levels are all ordered in the same way, meaning that for each factor, the level -1 is the X the further at the left, and the level 1 is the X the further at the right. Each X corresponds to the average of all the tests among the 48 which have the same level value. The factors are ordered on the x-axis, where ORIENT represents the channels and header orientation levels, POS and DIAM are, respectively, the inlet tube position and diameter, SPL is the splashing grid, INTR stands for tube intrusion, and finally WAT and AIR corresponds to the water and air inlet flow rates. Looking at the variability of the response for different levels of each factor, the most affecting parameters can be assessed. The average of the 48 STD_{water} values is represented on the graph by the horizontal dashed line.

In line with the results by Dario et al. during their review on this topic [4], the factor with the highest influence of the flow distribution is the channel and header orientation ORIENT. It is recalled here that one should consult Table 3 and Figs. 2 and 3 for more information about the factors numbering and levels, as well the designation of the orientations. The first orientation HH-VDC shows by far the best results in terms of water flow uniformity among the eight channels. Then the second orientation HH-VUC obtains STD results a bit higher than the results of HH-VDC. The third orientation in terms of results is the VDH-HC orientation which obtains STD_{water} values a bit lower than the global mean STD value. Finally, the last orientations VUH-HC presents the worst water flow uniformity on average. This result clearly concludes that vertical channels and a horizontal header is preferable for a better flow distribution in the channels.

The large scale of the y-axis of Fig. 11(Top), due to the great impact of the orientation, does not give a high visibility on the best selection for the other factors. Fig. 11(Bottom) displays the same information as Fig. 11(Top) but without the orientation factor, for a clearer visualization of the other parameters influence. The second most influencing parameter is the inlet tube position, followed rather closely by the inlet water flow rate. The rest of the factors, meaning the inlet pipe diameter, the presence of the splashing grid, the tube intrusion and the air flow rate have a similar and lower impact of the water distribution. Nevertheless, the channel intrusion is found to improve overall the flow distribution, and this improvement increases as the intrusion increases. It is however important to highlight that this ranking and conclusions are valid for the overall study. For each header and channel orientation, a different ranking of parameters of influence could be established as will be highlighted in Section 5.4.

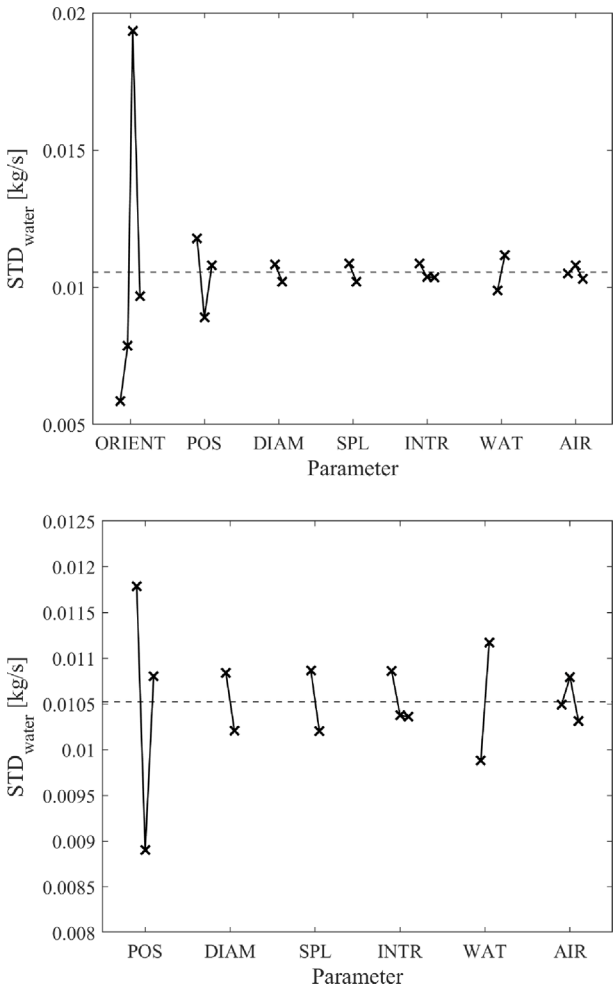

Fig. 11. (Top) DOE Mean plot of the 48 runs, (Bottom) Mean plot of the 48 runs without the orientation.

5.1.2. Best expected combination

From Fig. 11, an indication of the best combination of parameters is obtained. As previously stated, the response was defined as the standard deviation across all channels of the individual water flow rate. Thus, the optimal configuration is the setting that minimizes the STD_{water} response: it is expected for a HH-VDC orientation, a perpendicular lateral inlet position, with the greatest inlet tube diameter, with the splashing grid, with the highest channel intrusion, with the lowest water and the highest air flow rates. This set of parameters does not corresponds to a configuration of the test matrix. However, the STD results for the intrusion of 33 mm and 66 mm are close. Thereby, the flow distribution from another similar test, with a channel intrusion of 33 mm and giving very low STD values can be examined to get an insight of the possible water flow distribution profile of the best expected configuration. A visualization of the header during this specific test is displayed in Fig. 12, together with the water phase distribution among the channels. This test however corresponded to a parameter combination without the splashing grid. The outlet of the test section is located next to the channel 8. Nevertheless, as one can see, the water phase distribution is remarkably homogeneous among the eight channels. Channels 1 and 2 tends to be slightly underfed by the water for all conditions due to their location that faces the feeding tube: the perturbation at the surface of the pond is the greatest at their direct surroundings leading to a lower local level of the water. This uniform distribution is due to several phenomena. Firstly, the perpendicular large tube inlet diameter without the splashing grid delivers the air and water mixture inside the header

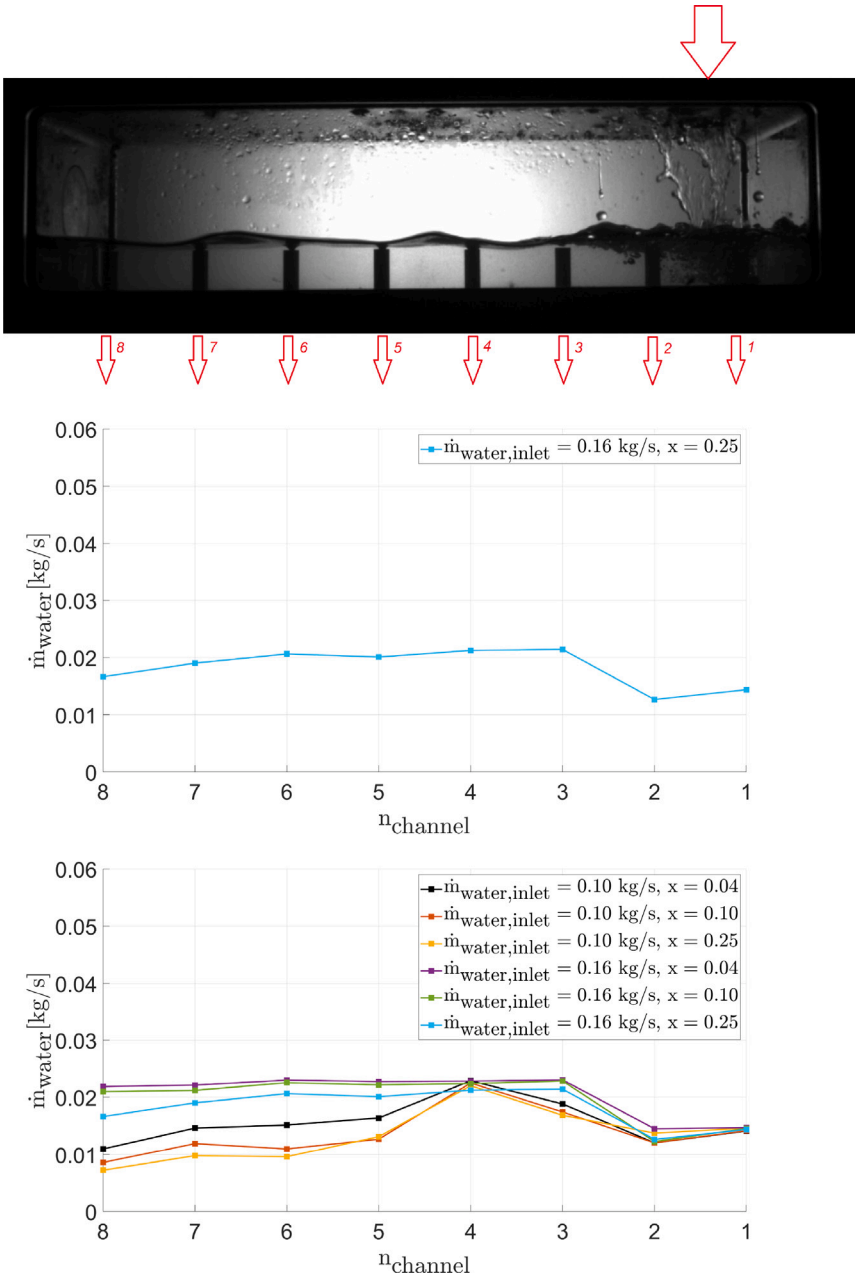

Fig. 12. Closest best expected combination: (Top) Visualization of the header, (Middle) Water phase distribution, (Bottom) Water phase distribution for all flow rate conditions tested.

as a smooth pouring such as a rain shower and not as a jet. Secondly, the tube intrusion creates a water pond at the bottom of the header. Thirdly, due to the low inlet velocities of the air and water phases, when meeting the water pond surface the inlet mixture creates shallow waves that agitate the water surface and propagate inside the whole header. As a consequence, the water is homogeneously distributed among the channels. This conclusion is verified for all the water and air flow rate conditions tested as can be seen in Fig. 12(Bottom).

5.1.3. Worst expected combination

The combination of parameters that is expected to produce the worst water phase distribution (i.e. leads to the highest response y) is the following: a VUH-HC orientation, a central and perpendicular to the header inlet, with the smallest inlet tube diameter, without the splashing grid, with no channel intrusion, with the highest water and the medium air flow rates. A visualization of the header as well as the water phase distribution among the channels for this configuration is presented in Fig. 13. A strong inhomogeneity in the water distribution profile is indeed obtained with this combination of parameters. The first three top channels are not fed with the liquid phase. Due to the low velocity of the two-phase flow entering the header through the perpendicular central inlet, the liquid reach is not improved and the liquid phase does not attain higher than the channel 4. Then, two substantial peaks of liquid overfeeding are encountered in the channels 6 and 8. The latter is the one closest to the outlet tube, and therefore represents a preferential pathway. This strong inhomogeneity in the water distribution profile is maintained for all the mass flow rates tested as can be seen in Fig. 13(Bottom). However, it is important to note that, as the inlet water flow rate $\dot{m}_{water,inlet}$ increases, so does the channel liquid reach. Indeed, for $\dot{m}_{water,inlet}$ of 0.10 kg/s, the channels from 1 to 4 are not fed by the liquid phase, while for $\dot{m}_{water,inlet}$ of 0.16 kg/s, the channels from 1 to 3 are not fed by water. Thereby, the liquid filling

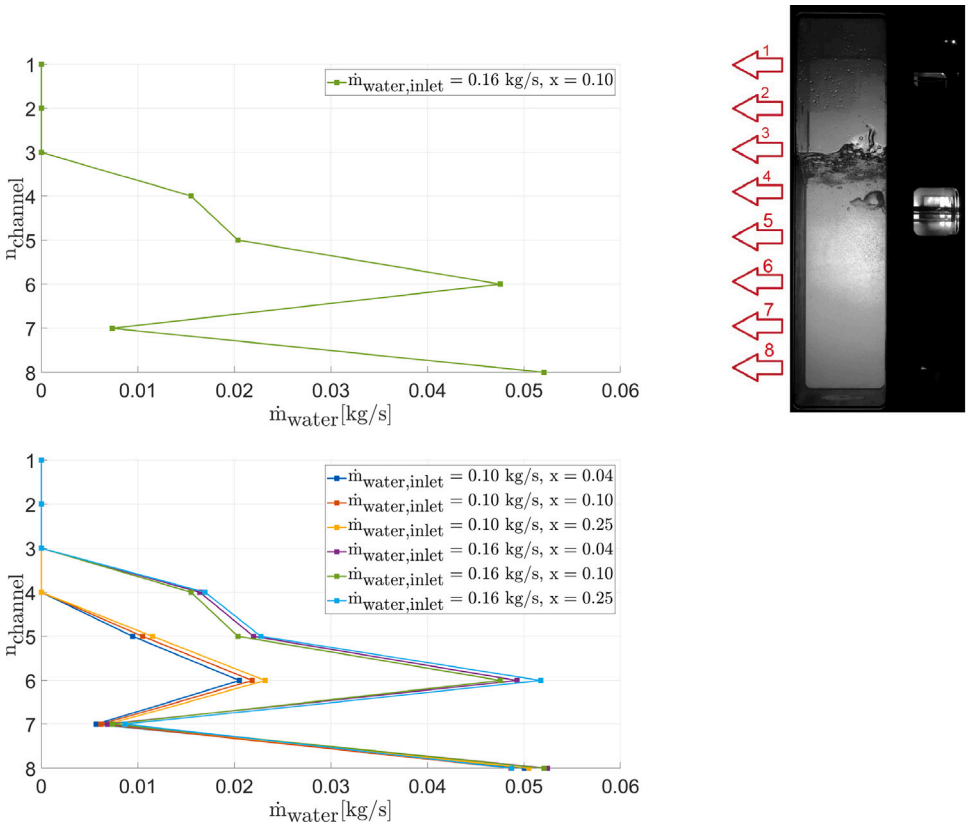

Fig. 13. Worst expected configuration: (Top-Left) Water phase distribution, (Top-Right) Visualization of the header, (Bottom) Water phase distribution for all flow rate conditions tested.

of the header increases as the inlet water flow rate $\dot{m}_{water,inlet}$ increases, improving the distribution.

5.2. Comparison with the literature: Main conclusions

5.2.1. Difficulty to form an annular flow

As already stated in Section 1.3, most experimental studies are performed with air and water at atmospheric pressure. However, as was highlighted by the work of Zou et al. [23], the fluid properties influences greatly the liquid distribution. They employed only refrigerants for their work (R245fa, R134a, R410A, and R32) that have phase density ratio $\frac{\rho_l}{\rho_v}$ of around 120, 80, 30 and 42 respectively. Nevertheless, they observed distribution coefficient varying for R245fa to more than double for R32 for various inlet conditions, and difference of tube liquid reach up to 25% between those two fluids. Thus, they demonstrated that the phase density ratio is an important parameter to consider when investigating the two-phase distribution problematic.

This is the reason why the applicability of the conclusions drawn from studies that exploits an air/water mixture at an atmospheric pressure as fluids to an actual evaporator using a refrigerant are very questionable. Indeed, at an atmospheric pressure and at a temperature of around 20 °C, the phase density ratio $\frac{\rho_l}{\rho_v}$ of air and water is as high as ~830. This is of an utterly different order of magnitude of what can be commonly encountered for refrigerants. As implied by Kim et al. in their future work [15], this totally changes the flow patterns encountered in the feeding tube and header. Indeed, since the magnitude and the distribution of the forces acting on the liquid and vapor phase are greatly transformed, the flow pattern transition are remarkably shifted.

In the present work, the phase density ratio $\frac{\rho_l}{\rho_v}$ is ~120 which is of the same order as the typical values for refrigerant fluids. Due to this density ratio similarity, the density of the air is risen from ~1.2 kg/m^3 to ~8 kg/m^3. The main repercussion of this rise is that the magnitude of the inertial forces is greatly diminished by comparison to tests that would have been performed at atmospheric pressure, while the magnitude of the gravitational forces is increased. Consequently, no annular flow could be reached neither for horizontal nor vertical upward inlet feeding tubes, not even at the highest qualities of x = 0.25 and in the feeding tube of smallest diameter in which the highest mass fluxes G of around ~513 kg/(s m^2) were reached. This is due to the inertial forces of the air that are not strong enough to push the water along the feeding tube walls. It should be however noted that annular regimes were observed in the vertical downward feeding tube of 23 mm diameter. The same conclusion for a horizontal inlet pipe is reported by Kim et al. [12]. They compared the results of the distribution among the 10 channels of a R134a flow and an air/water mixture flow obtained with the same set-up and test section, and operated at the same inlet conditions of mass flux G and quality x. They observed that even at quality x as high as 0.4, an annular flow pattern was reached for the air/water mixture, while the R134a flow produced only a stratified/stratified wavy flow. Therefore, this radically changed the distribution profile in their horizontal header connected to vertical downward channels. A similar study of Zhang et al. [22] led to the same conclusions: even at qualities as high as x = 0.35 for the R134a flow, no liquid film was reported on the top and side walls of the tube. Indeed, the absence of annular flow do not allow to create a forceful jet.

5.2.2. No forceful jet created

This conclusion is of paramount importance since most uniform distributions reported in the literature for horizontal header with vertical downward channels and vertical upward header with horizontal channels rely on the existence of such a jet from the feeding tube to push the liquid phase further away in the rear part of the header.

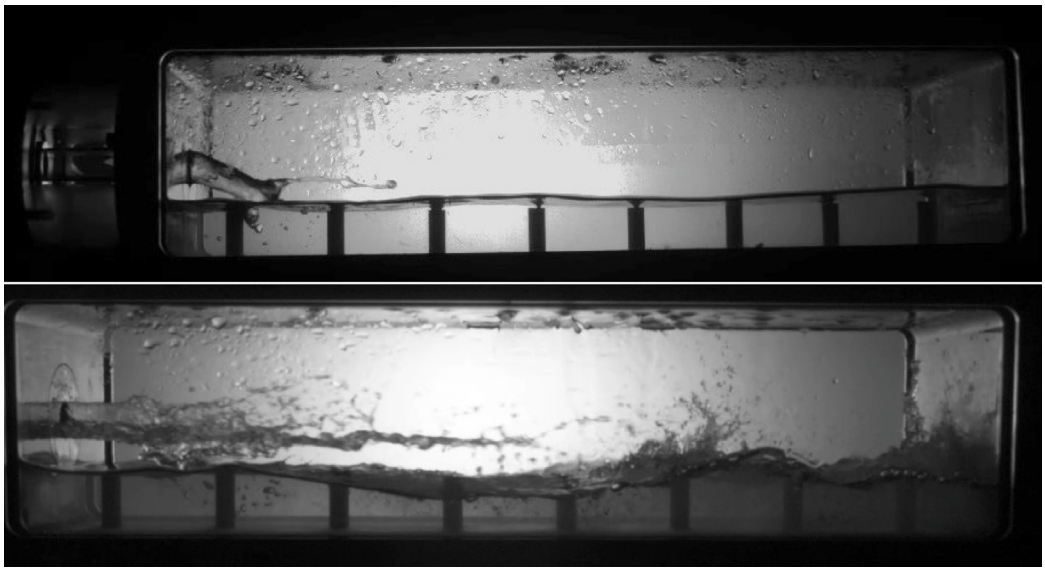

Fig. 14. (Top) Strongest jet observed in the 23 mm diameter horizontal inlet tube at quality $x = 0.21$ and total mass flux G = 357 kg/(s m^2), (Bottom) Similar test performed at atmospheric pressure condition and resulting jet observed in the 23 mm diameter horizontal inlet tube at quality $x = 0.10$ and total mass flux G = 317 kg/(s m^2).

Besides, this absence of jet changes also the behavior of the two-phase flow inside the header.

Horizontal header. It is widely reported in the literature [9,20], that for a two-phase flow entering a horizontal header with vertical downward channels, at low quality x and/or at low mass flux G, the liquid phase feeds mainly the channels located closest to the feeding tube. As x and/or G increases, due to the greater magnitude of the inertial forces a small jet is created, and the channels located further downstream starts to be fed as well. As the quality and/or mass flux are further augmented, a more powerful jet is enhanced. The channels located at the end of the header are fed with some liquid phase, and if the jet hits the wall of the rear part of the header, some recirculation occurs. Even if the transitions of all these flow structures differ between the work of Fei et al. [9] and Ahmad et al. [20] in term of liquid superficial velocity, the flow behaviors reported inside the feeding tube and the header are consistent.

With the difficulty to create such a liquid jet with the air and water at a pressure of 7 bar, the liquid phase could only feed the first channels in the present study. A picture of the strongest jet observed in the 23 mm diameter horizontal inlet tube is shown in Fig. 14. Even though this test makes use of a channel intrusion of $\frac{1}{4}$ of the header height, one can easily see that at quality $x = 0.21$ and total mass flux G = 357 kg/(s m^2), the jet created does not even reach the second channel. Without the intrusions in the example in Fig. 14, one could effortlessly conclude that the first channels only would be fed with the liquid phase. This would lead to a poor distribution.

Similar tests were performed for a HH-VDC orientation, a channel intrusion of $\frac{1}{4}$ of the header height, and a inlet tube diameter of 23 mm but at atmospheric conditions (i.e. ± 1 bar and 20 °C). An example of the resulting jet is shown in Fig. 14 (Bottom). For this test, the water mass flow rate was the same as in the example in Fig. 14, but the air mass flow rate was more than twice as small. Thereby, this jet is created for a quality of 0.10 and for a mass flux G = 317 kg/(s m^2). This confirms the expectations from the flow map study in Section 2.4.1. Indeed, the flow patterns observed in the feeding tube for the test conditions shown in Fig. 14 (Top) were mostly stratified or plug/slug. In contrast, intermittent to annular flow patterns were observed under the experimental conditions shown in Fig. 14 (Bottom) at lower quality. At a pressure of 7 bar, the volume of the air decreases significantly, making it difficult to reach the annular flow regime. As one can see in the header visualization of Fig. 14 (Bottom), the resulting jet at 1 bar is much powerful, even at a lower quality and mass flux, than the jet at 7 bar (Fig. 14). This strong jet at 1 bar reaches channels located up to the middle of the header, and the liquid surface is greatly disturbed by the two-phase flow jet.

Vertical upward header. Concerning vertical upward header, Lee et al. [7,40] tested an air and water flow in a 24 mm × 24 mm square header connected to 6 flat channels of 1.8 mm × 22 mm. They evaluated the influence on the distribution of total mass flux G ranging from 54 to 134 kg/(s m^2), of quality from 0.2 to 0.5 and different channel intrusion depths. They obtained a very good liquid distribution with a channel intrusion of $\frac{1}{8}$ of their header hydraulic diameter that was stable for three quality values of 0.25, 0.35 and 0.45 at a mass flux of 70 kg/(s m^2). However this uniform liquid distribution relies on the annular flow regime formed in the inlet tube, ahead of the header, that allows to form a strong liquid jet. Thanks to this jet, the liquid phase is able to reach and feed the top channels in the rear part of the header.

This is not what could be observed in the current study. Even at a quality of x = 0.33 and total mass flux of G = 570 kg/(s m^2), strong perturbations could be visualized at the interface between the liquid phase (water) and the gaseous phase (air) (see Fig. 15) due to the presence of bubbly and churn inlet flow patterns, but however no annular jet. As mentioned in the previous paragraph, the difficulty of reaching an annular flow pattern is due to the high density of the air generated by the 7 bar test condition, which is set to ensure a similar phase density ratio $\frac{\rho_l}{\rho_v}$ to that encountered for refrigerants. Consequently, the channels located at the top of the header were not fed by the liquid phase. This great horizontal phase separation is very similar to the observations shared by Redo et al. [41] of the behavior of a R410A two-phase flow in a rectangular header connected to 20 channels.

Due to the even higher vapor phase density of refrigerants, the difficulty to form a forceful jet in both a horizontal or vertical upward feeding tube at reasonable and representative quality and superficial velocities is expected to be higher. Thereby, the conclusions reported about great liquid distributions obtained by means of a jet in a horizontal or vertical upward header can be legitimately questioned. Indeed, it is unsure if these conditions can be replicated in an actual evaporator working with a refrigerant.

Fig. 15. Flow behavior inside the header with a 23 mm vertical upward feeding tube at a quality of x = 0.33 and total mass flux of G = 570 kg/(s m^2).

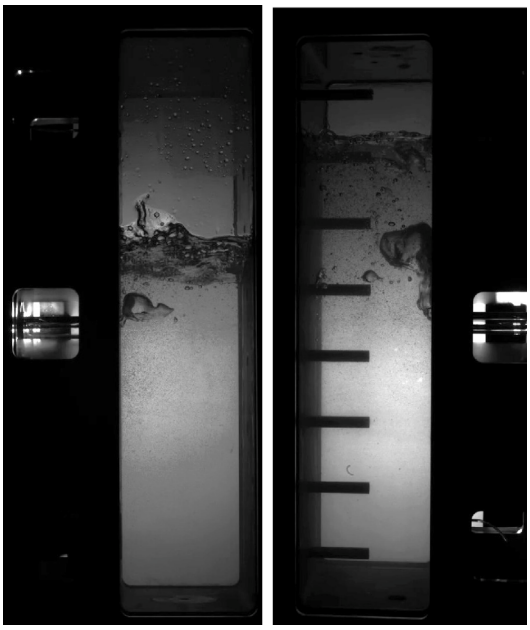

Fig. 17. Liquid height inside the header: (Left) for 23 mm perpendicular and horizontal feeding tube at the middle location and the outlet pipe located at the bottom in a vertical downward orientation, (Right) for 23 mm perpendicular and horizontal feeding tube at the middle location and the outlet pipe located at the top in a vertical upward orientation.

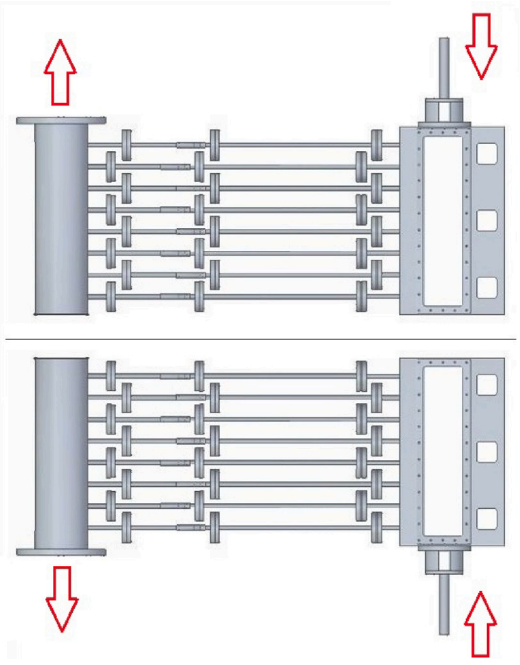

Fig. 16. Test section arrangement, outlet location and two-phase flow path for a: (Top) Vertical downward header, (Bottom) Vertical upward header.

5.2.3. Importance of outlet tube in vertical header orientation

As indicated in Section 2.2, the simplified evaporator was always operated in a "U" shape, meaning that the inlet and outlet pipes were located on the same side as shown in Fig. 3. As a consequence, when the test bench was installed with a vertical upward header orientation, the outlet pipe was located at the bottom of the exit collector in a downward direction (see Fig. 16(Bottom)). Conversely, with a vertical down header orientation, the outlet pipe was located at the top in an upward direction (see Fig. 16(Top)). For both vertical upward and downward header orientations, the middle and perpendicular inlet feeding tube positions were tested. Thereby, for a similar inlet tube position and diameter, the direct impact of the outlet location can be analyzed. These configurations are presented in Fig. 17, for which the two-phase behavior inside the header is presented for two different tests. Between these two tests, both inlet feeding tube are located at the middle position and are perpendicular to the header. The inlet tube diameter is in both cases of 23 mm diameter and the inlet air and water conditions are almost identical: the inlet quality is 0.30 and the inlet total mass flux is ~ G = 500 kg/(s m^2) with less than 10% of difference between these two tests. However, one meaningful difference lies in the outlet pipe location. As can be straightforwardly noticed from Fig. 17, the liquid height inside the header at the right is significantly greater than the one inside the header at the left. For the configuration in Fig. 17(Right), the outlet pipe was located at the top of the collector exit (see Fig. 16(Top)). This top location leads to an important filling of the header by the liquid phase, as some substantial hydrostatic pressure losses to overcome by the two-phase flow appear in this arrangement. Consequently, one can safely conclude that the outlet location is an impacting parameter in the case of a vertical header and that a top exit location is able to increase the liquid reach inside the header to feed highest channels. It is thus to be preferred. This strong header filling due to a top location of the outlet pipe is also reported in the work of Zou et al. [42] with R134a. However, this outlet tube location is not mentioned in the literature [4,5] as a major parameter impacting the distribution, as it is little studied. Thereby, this parameter was not selected in the DOE in the present work. Nevertheless, thanks to this comparison, an insight about its impact for vertical headers is obtained. This parameter is however believed to impact much less the distribution for horizontal headers.

5.2.4. Header strongly filled with the liquid phase for a HH-VUC orientation

Even at qualities x of around ~0.25–0.3 and in the absence of channel intrusion, an almost complete filling by the liquid phase of the horizontal header connected to the vertical upward channels is

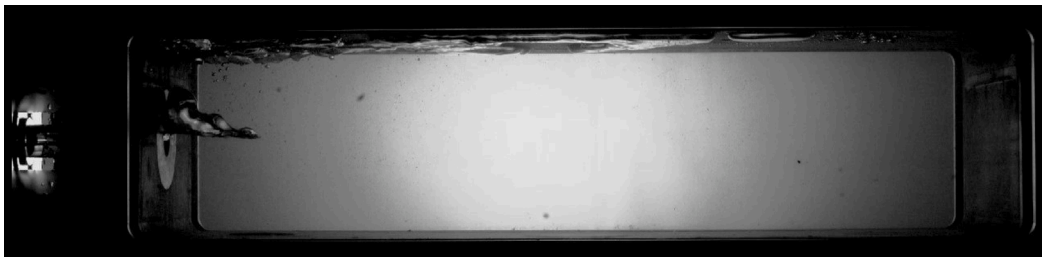

Fig. 18. Example of the two-phase flow behavior inside the horizontal header connected to the channels oriented vertically upward.

observed (see Fig. 18). This behavior is very similar to what has been reported by Ahmad et al. [20]. Indeed, from quality values of 0.0.5 to 0.2, they reported that the vapor phase begins to occupy a very small volume inside the header and is mainly present as a bubbly regime in the upper part of the header. In the present work, as soon as the air exits the feeding tube, this gaseous phase gathers against the top wall of the header, and occupies a tiny portion of it. This is very likely due to the pressure test condition of ~7 bar. In fact, as the air density increases due to the pressure increase, the volume of the air decreases accordingly.

5.3. Impact of combined parameters

As stated in Section 1, the main gap that still exists in the literature is to understand the impact of several parameters combined. Some combinations of two parameters have been properly addressed in the literature. However, the influence of several combinations of parameters lacks in the literature and especially when it comes to comparing more than two parameters, such as the inlet and outlet tube combined positions together with the header and channel orientation for example. Besides, as explained previously in Section 5.2, most studies were carried by exploiting an air and water mixture at atmospheric conditions as fluids, which is a significant limitation.

To compare the effects of three parameters combined is not an easy task. The block plot is graphical tool able to assess the effect of 3 combined variables can be assessed, and the interaction between specific and targeted levels of factors can be analyzed. It allows the evaluation of whether a parameter of interest (*primary parameter*) has a statistically significant effect on the response and whether its influence follows the same trend over all the *secondary parameters* and *tertiary parameters*. It shows the STD_{water} (y-axis) as function of all combinations of all levels of secondary factors (x-axis), while the primary factor of interest is displayed with symbols of different colors depending on their levels. The most explanatory block plots are shown in Figs. 19–21. All the STD_{water} are displayed with a X mark.

The way of understanding a block plot will be shown on the example of Fig. 19: the channel intrusion is examined as *primary parameter*; the different colors of the *cross* marks indicate its different levels. On the x-axis, the first 3 columns are relative to the 3 possible inlet tube position levels specific to the channel and header orientation −1 (HH-VDC). The same occurs for the columns 4, 5 and 6 with orientation $-\frac{1}{3}$ (HH-VUC), and so on. Besides, it is recalled that the test conditions and the combination of parameters leading to the best liquid phase distribution are found for the lowest STD_{water} (y-axis) response. As the gravity force acts differently on the air/water mixture for each orientation, a general and common trend of the combination of the intrusion, inlet tube position and diameter, and the splashing grid for all orientations is inconceivable. Thereby, the header and channel orientation will serve as reference parameter for all the comparisons. Besides, as explained in Section 2.3, for each of the 48 runs selected by the algorithm, the 6 combinations of water and air levels in total were tested. To efficiently compare the influence of the combined parameter through the block plots, the response of these 6 test points was utilized.

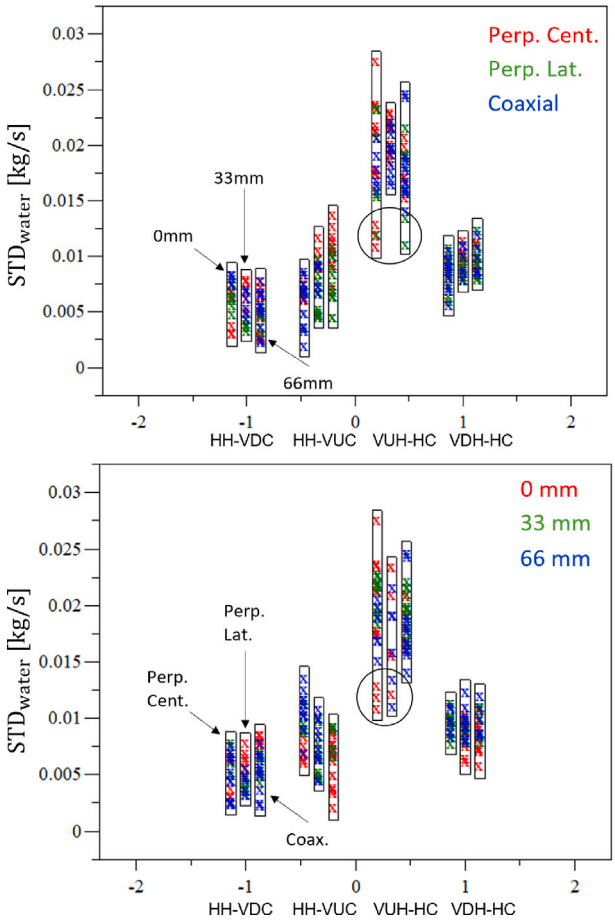

Fig. 19. Block plots of the combined interaction of: (Left) orientation, channels intrusion and inlet tube position, (Right) orientation, inlet tube position and channels intrusion.

5.3.1. Combination of orientation, position and intrusion

The combined effect of header and channel orientation, feeding tube position and channel intrusion is shown in Fig. 19. Overall, the lowest STD_{water} values for the HH-VDC orientation. For this specific orientation, very similar distribution results are obtained for whatever combined levels. This is seen in the equivalent range of the response for the three bars, which indicate that the effect of intrusion levels is low. Nevertheless, one can observe in Fig. 19 (Right) that for both perpendicular lateral and coaxial inlets combined to a HH-VDC orientation, the presence of at least a 33 mm intrusion improves significantly the liquid phase distribution. Additionally, for a perpendicular central inlet combined to a 66 mm intrusion, a cluster of test points displays a very uniform distribution. However, with no intrusion the coaxial inlet presents the worst liquid distribution as reported in the literature [4,

5], while the perpendicular central one displays the best results and especially when combined with a tube intrusion of 66 mm.

For HH-VUC orientation, a sharp noticeable trend can be observed. Indeed, as the channel intrusion increases, the STD_{water} values increases. Thus, the channel intrusion for this header and channel orientation worsens the liquid distribution. Besides, the perpendicular central inlet when combined to whatever intrusion level leads to the worst liquid distribution in this orientation. On the other hand, the coaxial inlet position is to be preferred as it leads to the best liquid distribution.

For VDH-HC orientation, a similar trend but of lesser amplitude to what has been observed for a HH-VDC orientation can be noted: as the channel intrusion increases, the liquid flow distribution worsens. Furthermore, the coaxial inlet position is also to be slightly preferred.

Finally, for certain combinations of levels, some of the test points stand out from the others and present much lower or higher values of STD_{water}, leading to a very wide range of liquid distribution response. For instance, it is quite difficult from this graph to conclude about the combined effect of a VUH-HC orientation, the inlet tube position and the channel intrusion. Indeed, in this orientation, a perpendicular central inlet combined to an absence of intrusion (0 mm) shows a group of some low STD_{water} values but on average does not lead systematically to a great distribution. The same situation is encountered for a VUH-HC orientation again, but combined to a perpendicular lateral inlet and a channel intrusion of 66 mm, that display a cluster of a few data points with low STD_{water}. These two examples are circled with a solid black line in Fig. 19 to highlight them. It can mean that these specific points exhibit low STD_{water} values due their combination with a fourth and even a fifth parameter level. By crossing the information given by three figures, these levels can be identified. Nevertheless, it seems that a coaxial inlet is to be avoided for this orientation since it leads to less uniform distribution.

5.3.2. Combination of orientation, intrusion and diameter

The impact on the STD_{water} of the combination of the header and channel orientation, the feeding tube diameter and the channel intrusion is displayed in Fig. 20. For a HH-VDC orientation, it is rather hard to draw a sharp conclusion on the combined influence of the tube intrusion and the inlet feeding tube diameter. However, it can be pointed out that a larger feeding tube diameter (56 mm) seems to improve the liquid phase distribution when combined to a 33 mm channel intrusion, while it worsens the distribution in case of an absence of intrusion (0 mm). When comparing these tests points to the previous Fig. 19(Left), it appears that they are related to a perpendicular lateral inlet and a coaxial inlet respectively. Thereby, as already reported in the literature, a coaxial feeding tube of large diameter for a HH-VDC orientation and no intrusion is to be avoided (see Section 1.1). Similarly, for a VUH-HC orientation, no straightforward conclusion can be drawn. There is indeed a mixed influence of the feeding tube diameter when combined to the channel intrusion for this orientation. However, when comparing Fig. 20(Left) with the previous Fig. 19(Left), it can be concluded that the clusters of point circled for the VUH-HC orientation combines firstly a perpendicular central inlet combined to an absence of intrusion (0 mm) and an inlet tube diameter of 56 mm, and secondly a perpendicular lateral inlet, a channel intrusion of 66 mm and an inlet tube diameter of 23 mm.

For a HH-VUC orientation however, the conclusion is far more obvious: a smaller feeding tube diameter of 23 mm leads to a better liquid phase distribution, for all the three intrusion depths studied. Likewise but with a small extent, for a VDH-HC orientation, overall, a smaller feeding tube diameter helps the distribution. This is particularly true when combined to an absence of intrusion (0 mm).

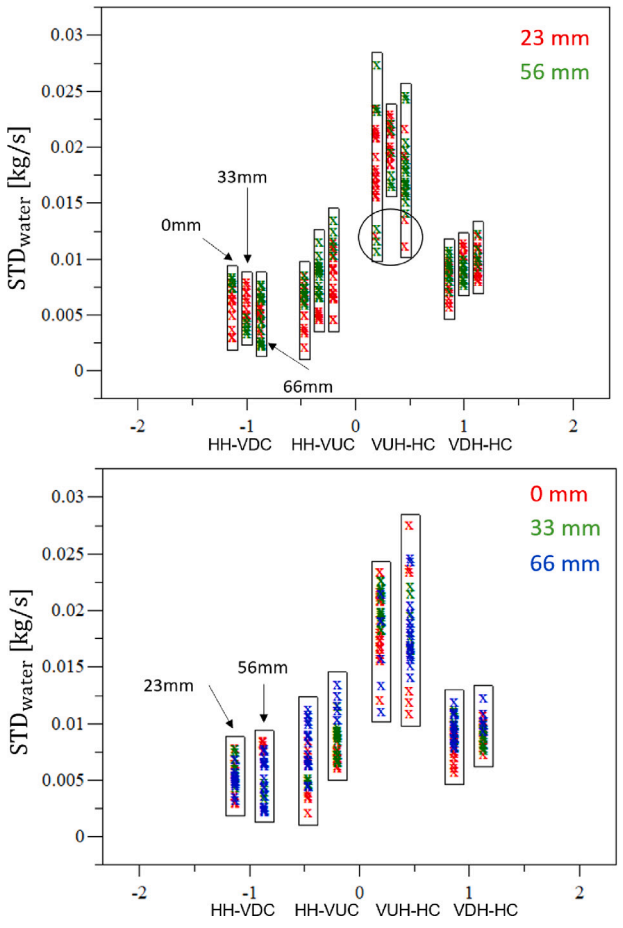

Fig. 20. Block plots of the combined interaction of: (Left) the orientation, the channels intrusion and the inlet tube diameter, (Right) the orientation, the inlet tube diameter and the channels intrusion.

5.3.3. Combination of orientation, position and splashing grid

The combined influence of the header and channel orientation, the feeding tube position and the splashing grid on the liquid phase distribution is displayed in Fig. 21. In general terms, the presence of the grid does not unfortunately lead to a great and striking improvement of the distribution (see Fig. 21(Right)), apart in the case of a HH-VUC orientation. For that specific orientation, the presence of the grid greatly help to homogenize the liquid phase distribution when combined to both a perpendicular lateral inlet position and especially to a coaxial inlet position. It should however be pointed out that the splashing grid was mainly expected to enhance the distribution for horizontal pipes by breaking the stratified flow regimes, which are usually leading to the least uniform distribution. Nevertheless, even when considering only the horizontal pipes (HH-VDC and coaxial inlet, VUH-HC and VDC-HC with both perpendicular lateral and central inlets), no sharp improvement of the distribution seems to be obtained thanks to the grid.

5.4. Summary and design rules per orientation

The purpose of this section is to help the reader by summarizing the findings and to recap the main design rules of what improves the flow distribution for each of the four orientations tested.

5.4.1. Horizontal header and vertical downward channels

For this header and channel orientation, the gravity acts in the direction of the flow. Therefore, as soon as the two-phase flow exits the

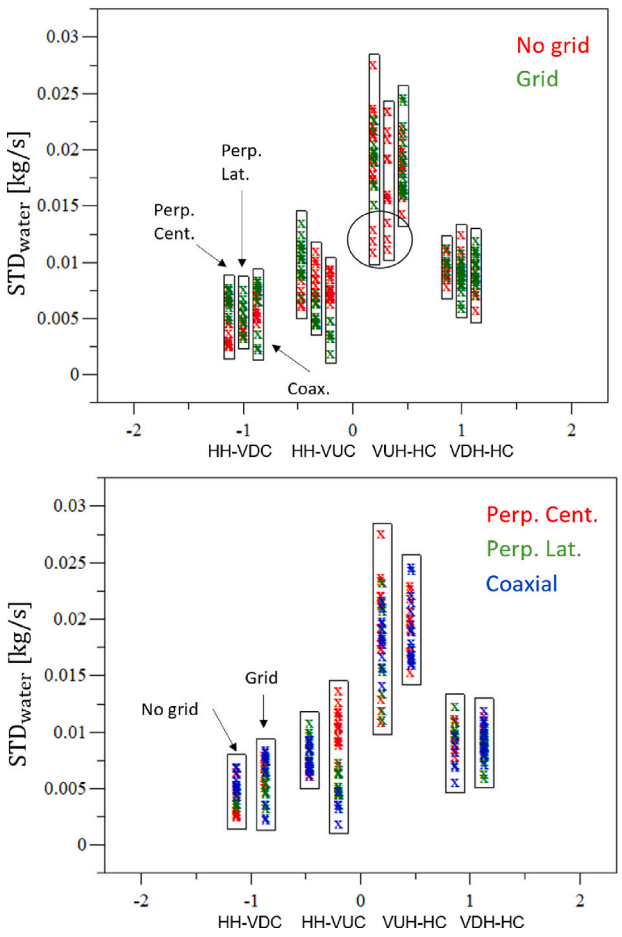

Fig. 21. Block plots of the combined interaction of: (Left) the orientation, the channels tube position and the presence/absence of the splashing grid, (Right) the orientation, the presence/absence of the splashing grid and the inlet tube position.

feeding tube, the liquid phase tends to falls down directly onto the bottom wall of the header, feeding only the first channels close to the inlet. For this reason and as already largely highlighted in the literature [4,5], a coaxial inlet of large diameter is to be avoided when targeting an homogeneous distribution in this orientation. On the other hand, this study confirmed that a channel intrusion of $\frac{1}{4}$ (33 mm) or $\frac{1}{2}$ (66 mm) of the header height enhances the distribution, especially combined to a coaxial or perpendicular central inlet of 56 mm diameter. The best distribution for this specific orientation in the present work is found for a channel intrusion of $\frac{1}{2}$ (66 mm), together with a perpendicular central inlet of the largest diameter (56 mm). An example of the two-phase flow behavior inside the header can be visualized in Fig. 22 as well as the liquid phase distribution profile inside the channels for the 6 combined air and water test conditions. The water flow distribution is found to be very homogeneous over the whole range and air and water flow rates tested. This result is similar to the distribution presented in Fig. 12. However, with the 66 mm intrusion, the liquid/gas interface is located further away from the bottom wall of the header and waves of higher amplitude can be created. Besides, in that specific orientation, the central position of the feeding tube allows for a better spreading over all the eight channels. This combination of parameters for this header and channels orientation was never tested in the literature to the author's best knowledge, and thus was never identified as enabling a uniform distribution.

5.4.2. Horizontal header and vertical upward channels

For this orientation, the gravity acts against the direction of the flow, and this especially important for the water phase because of its high density. A channel intrusion is not recommended for that channel and header configuration as discussed in Section 5.3.1. Indeed, the channel intrusion results in this case of the opposite phenomenon of the one occurring in the HH-VDC orientation: the intrusion leads to the creation of a gas pocket. An example of a visualization is shown in Fig. 23 for a channel intrusion of 66 mm as well as the corresponding water distribution among each of the eight channels. A parabolic profile can be observed of the water feeding. The channels facing the inlet feeding tube receive around three times more of the liquid phase when compared to the other channels. Besides, as the inlet water mass flow rate increases, the width of the parabolic profile increases. A reverse flow situation can be noticed in the channels 7 and 8.

Besides, as already highlighted in Section 5.3.1, the maldistribution increases as the tube intrusion increases. The reason for this straightforward consequence is the direct volume growth generated of the gas pocket. Indeed, as it grows, the gas/liquid interface is located further away from the top walls of the header, enhancing waves of higher amplitude at this interface when the two-phase flow enters the header. The feeding of the tubes becomes more unstable and periodic, deteriorating the liquid distribution. A similar strong phase separation was observed by Byun et al. [43] and Kim et al. [44] for R134a in the same header and channel configuration. Kim et al. [44] as well observed that the channel intrusion led to a deterioration in the distribution when compared to flush-mounted channels. This effect is even more pronounced with a perpendicular central inlet. Indeed, for the two other inlet positions (Perpendicular lateral and coaxial), their location at the extremities of the header allows a diminution along the header length of the gas/liquid interface perturbation generated by the two-phase flow exiting the feeding tube. The perpendicular central position however does not allow for sufficient diminution, and thus the two other inlet positions are to be preferred. Lastly, both a feeding tube of smaller diameter and the presence of the splashing grid improves the liquid distribution, and this is especially the case when combined to a coaxial inlet. This can be explained as they both increase the two-phase flow velocity and allow inertial forces to increase in magnitude. The best liquid distribution is indeed encountered in this orientation for such combination of a tube inlet diameter of 23 mm and the presence of splashing grid. Besides, the inlet position is coaxial and there is no channel intrusion. A header visualization is shown in Fig. 24 as well as the water distribution for each test condition.

As can be observed, the two-phase flow jet reaches the channels located further away from the entrance. Even though the first channels located near the inlet tend to be overfed by the liquid phase, the distribution profile displays a smooth and rather uniform trend for all flow condition tested. Besides, the water distribution improves as the inlet quality and water mass flow rate increase.

5.4.3. Vertical upward header and horizontal channels

From the figures presented in the previous Section 5.3, it appears difficult to draw design rules and conclusions for this orientation. For instance, no sharp trend between the intrusion, the orientation, and the feeding tube position can be found. There is also a mixed influence of the inlet tube diameter on the distribution. Thereby, no general rules can be derived from these conclusions. Some more uniform distribution are however found but they concern very specific combinations of parameters, which highlight again the need of such systematic study and the great help provided by the Design of Experiment algorithm to select the test matrix. The presence of the grid seems however to worsen the distribution, because the best distributions are found without the grid. Overall, this study shows the highest values of STD_{water}, and so the worst distribution, for this header and channels configuration. The main problem with vertical headers and vertically downward oriented outlet tube is the lack of liquid phase feeding to the upper channels,

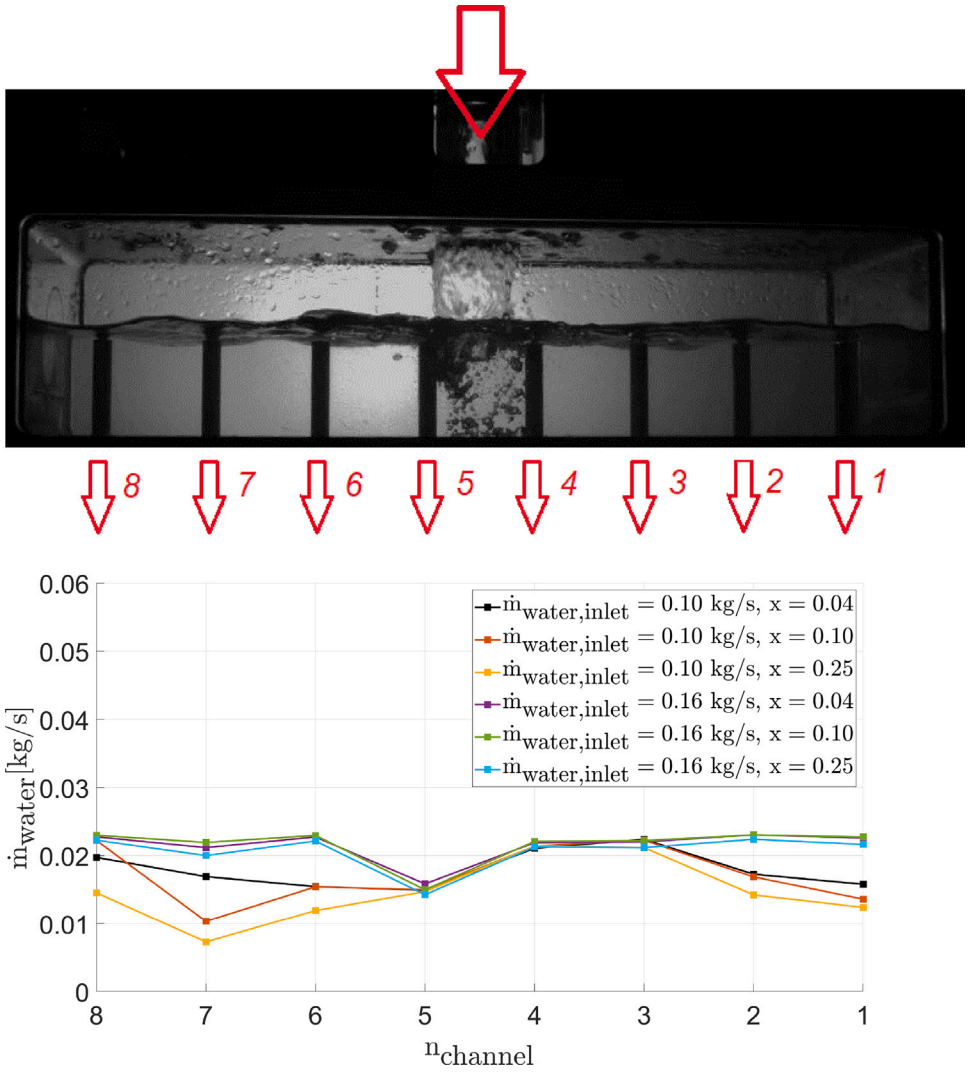

Fig. 22. Most homogeneous water phase distribution obtained for a HH-VDC orientation for all flow rate conditions tested.

while the lower channels are always supplied with liquid phase. The solution to obtain more uniform distributions then lies in finding ways to feed the top channels. A perpendicular lateral inlet and 66 mm of channel intrusion seems a good way of achieving such feeding as can be seen in Fig. 25. This combination of parameter, without the splashing grid and with the 23 mm feeding tube, leads to the best water phase distribution obtained for a VUH-HC orientation. Indeed, as one can observe, the header is about half filled with the liquid phase and this level increases as the water mass flow rate increases. Therefore, all the channels below this liquid reach are greatly fed with water. Due to the perpendicular lateral inlet, the two-phase flow jet exiting the feeding tube, even if not powerful, is able to supply the other channels that are above the liquid reach, thanks to the inlet position combination with the 66 mm channel intrusion. Even if the distribution obtained cannot be considered as uniform and desirable, this combination of parameters enables a better feeding of the liquid phase in the channels. The channel 1 is however never fed by the water. Besides, a water recirculation is detected in the channel 7 for a few test conditions, that tends to disappear as the quality increases.

5.4.4. Vertical downward header and horizontal channels

In this header and channel orientation, due to the outlet tube being oriented vertically upward, the header is greatly filled with the liquid phase. Besides, due to the vertical orientation of the header and as already mentioned, the hydrostatic forces to overcome by the two-phase flow are substantial. Therefore, the various parameters tested do not tremendously impact the distribution which impedes significant improvements concerning this orientation. Nevertheless, it is still possible to draw a few conclusions about the influence of the parameters. For instance, it appears that as the channel intrusion increases, the liquid phase distribution worsens, for whatever other parameters it is combined with. Besides, a smaller inlet tube diameter is to be preferred, especially when combined to a coaxial inlet. A small inlet indeed enhances the magnitude of the inertial forces of the two-phase flow and creates strong perturbations at the air/water interface. This generates movement of this interface which can improve the liquid reach and thus enable the feeding of the upper channels. However, the impact of the inlet position is less important than the intrusion and the inlet tube diameter. Indeed, a perpendicular lateral inlet combined with 0 mm of intrusion also lead to some lower values of STD_{water}. No trend about the influence of the grid could be however assessed. Nonetheless, a slightly better distribution could be obtained for two combinations of parameters. The first one is obtained for a small coaxial inlet of 23 mm and with no grid nor channels intrusion. The second one is obtained with a small perpendicular lateral inlet of 23 mm and with no intrusion. For this second combination, the water flow rate distribution is displayed in Fig. 26, as well as a visualization of the flow behavior inside the header. As one can observed, the distribution displays, for all water and air mass flow rate conditions tested, two peaks of liquid

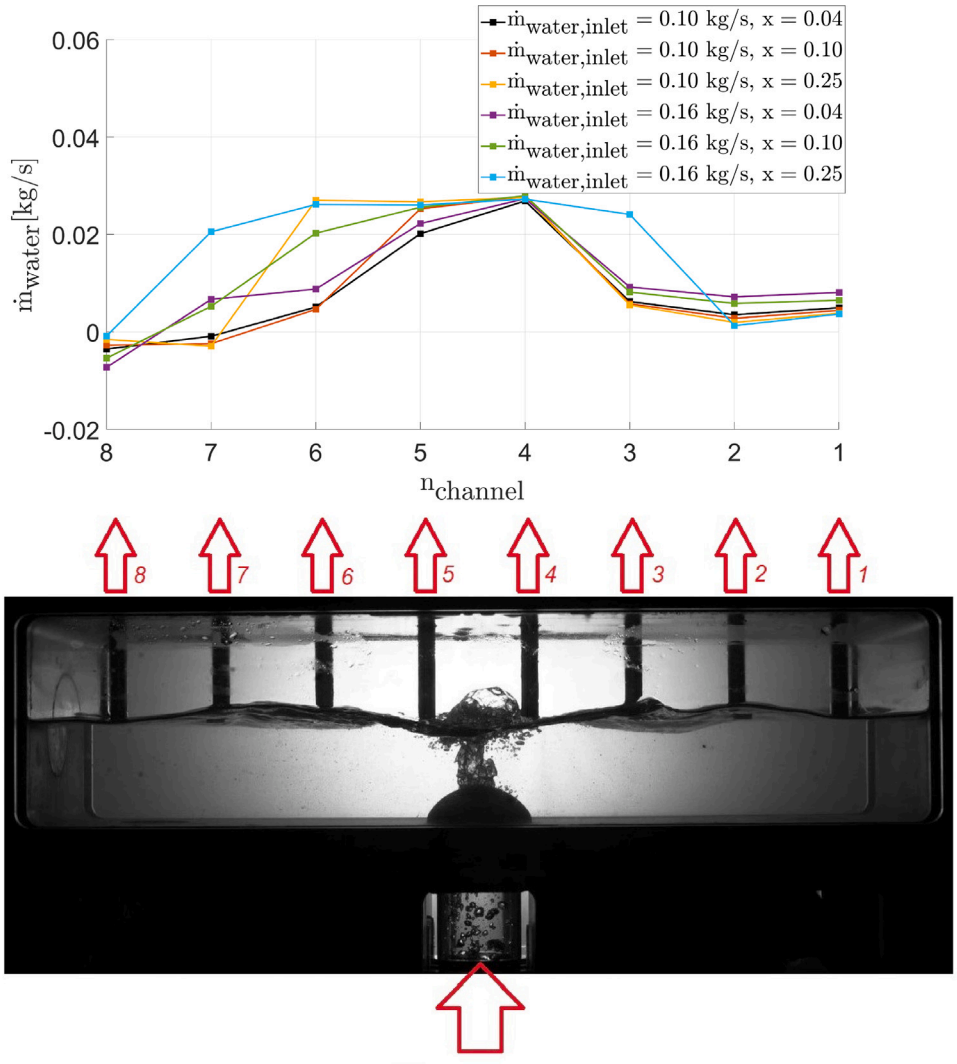

Fig. 23. Water phase distribution obtained for a HH-VUC orientation for all flow rate conditions tested and for a channel intrusion of 66 mm.

Table 5
Influence on the two-phase distribution of the various parameters studied presented per orientation.

Orientation	Inlet Pos.			Diameter		Grid		Intrusion			Outlet pos.
	Perp. Central	Perp. Lateral	Coax.	23 mm	56 mm	Pres.	Abs.	0	$\frac{1}{4}$	$\frac{1}{2}$	
HH-VDC	++	+	–	+	–	/	/	––	+	++	/
HH-VUC	––	–	++	++	–	+	–	+	–	––	/
VUH-HC	–	+	–	+	–	–	+	–	–	+	++
VDH-HC	–	–	+	++	–	/	/	+	––	––	++

overfeeding, in the channel 4 and especially in the channel 7. This is due to the fact that the channel is the second closest to the test section exit, the first being the channel 8 which is never fully immersed. Indeed, due to the vertical upward orientation of the outlet pipe in this configuration, the header is almost filled with the water phase, leaving to the air a small pocket at the top. Thus, the hydrostatic pressure induced by this water volume is high, as well as the pressure drops to overcome for the air and water mixture to exit the test section. Consequently, due to its close location to the outlet, the channel 7 represents a clear preferential pathway for the water flow.

5.4.5. Summary conclusion

To conclude this summary of design rules per orientation with more visual guidelines on which parameters and levels improve and worsen the distribution, Table 5 is proposed.

6. Conclusion

This study conducted an experimental investigation into the multi-factorial effect of various parameters on the two-phase flow distribution within the simplified version of an evaporator header. Total mass fluxes G spanned from 42 kg/(s m^2) to 513 kg/(s m^2). Three inlet qualities were targeted: 0.04, 0.1 and 0.25. The experimental tests were carried with air and water in flow pattern similarity with a low GWP refrigerant, at a pressure operating condition of 7 bar, at room temperature and at isothermal conditions. Four orientations of the header and channels were examined. The feeding tube could be moved to three different positions and its diameter varied (23 mm or 56 mm). Different channel intrusions into the header height were as well tested: 0, $\frac{1}{4}$ and $\frac{1}{2}$. Lastly, a splashing grid could be placed at the entrance of the header to

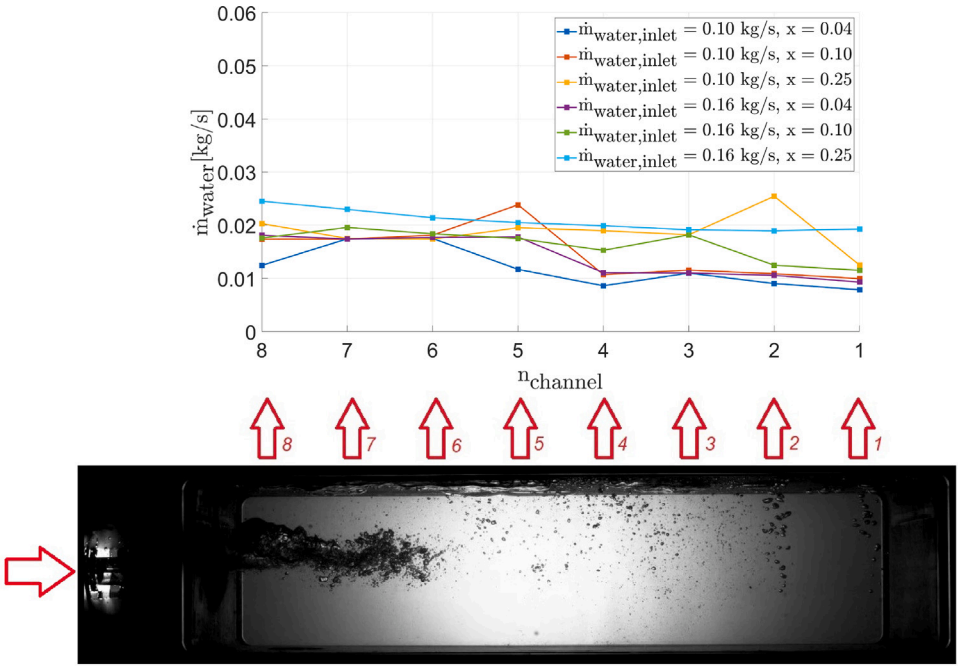

Fig. 24. Best water phase distribution obtained for a HH-VUC orientation for all flow rate conditions tested.

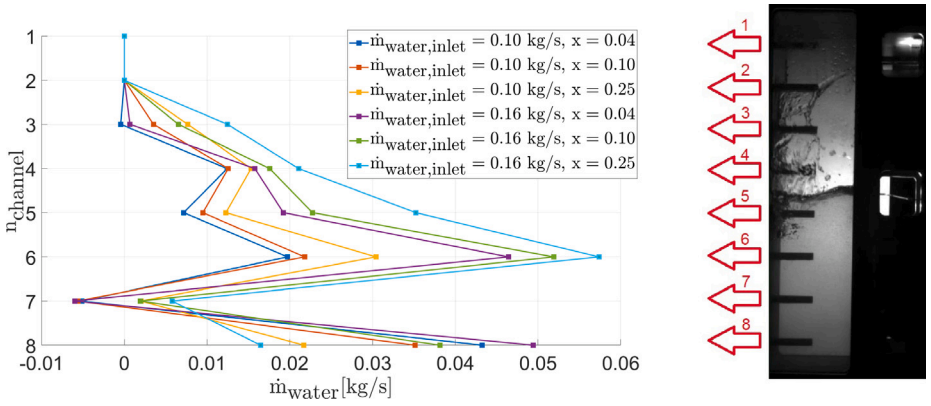

Fig. 25. Best water phase distribution obtained for a VUH-HC orientation for all flow rate conditions tested.

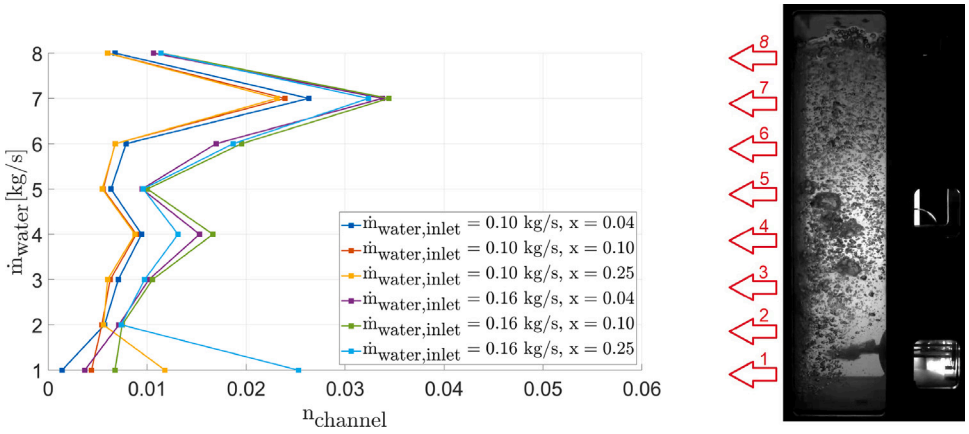

Fig. 26. Best water phase distribution obtained for a VDH-HC orientation for all flow rate conditions tested.

modify the inlet flow pattern. A Design Of Experiment (DOE) technique was employed to construct an optimized test matrix. Forty-eight tests were deemed necessary. The results between each configuration were compared using the standard deviation of the water flow distribution.

The orientation is found to be the most impacting parameter. The inlet tube position also showed a substantial impact on the distribution, before the presence of the splashing grid, the inlet tube diameter and the channel intrusion. The best water phase distribution is expected to be for a HH-VDC orientation associated to a perpendicular lateral inlet position and largest inlet diameter, with the splashing grid and the highest channel intrusion, and for the lowest water and the highest air inlet flow rates. This combination of parameter has not be tested, but the water distribution profile of the test with the closest combination displayed a greatly uniform distribution with the entire range of inlet flow conditions, which confirms the expectation. The worst distribution is expected for a VUH-HC orientation coupled to a perpendicular central inlet of smallest diameter, without the splashing nor intrusion, and for the highest level of water medium level of air. This combination of parameter has been tested and the water distribution indeed displayed a highly uneven feeding among the channels, verifying again the predictions. Besides, overall, the worst water distributions were found for a VUH-HC orientation.

The flow maps predicted a great shift in the flow pattern due to the pressure necessary for the flow pattern similarity. This is confirmed by the experimental tests. There is a difficulty to form an annular flow and to increase the inertial forces of the flow due to the high density of the air. When compared to the literature, this is of great disadvantage since most uniform distributions reported in the literature rely on acceleration of the two phase flow and the formation of an annular flow pattern.

The study showed in the case of a vertical header the difficulties to find efficient ways to improve the distribution. It was indeed arduous to draw sharp conclusions about the various combinations of parameters tested and few clear trends could be defined for both vertical headers configuration. However, the position of the outlet tube and its direction showed a straightforward impact on the liquid filling of the header. On the other hand, for both horizontal header configurations, some clear and interestingly opposite trends could be obtained. The channel intrusion proved to successfully enhance the distribution for a HH-VDC orientation while it worsens it for a HH-VUC orientation. A coaxial inlet position is advised for a HH-VUC orientation while it is to be avoided for a HH-VDC orientation. Lastly, great distributions could be achieved for several combinations of parameters for these horizontal header configurations, that were besides stable over all the air and water flow rate tested.

Thanks to this experimental work and with the help of the design of experiment, a great contribution to the understanding of the liquid phase distribution inside an evaporator header is brought. With the two-phase flow pattern similarity, these findings can be transferred to an evaporator operating with a refrigerant. Besides, several combinations of parameters that were not yet tested in the literature could be identified. Some of them, such as the combination leading to the best distribution obtained for a HH-VDC orientation led to very uniform water distributions. However, due to the limitation to 48 runs, the influence of all the interactions are not obviously available but some deep insights were already obtained about the two-phase flow behavior inside a header.

As a future work, a similar DOE study will be achieved on a real scale evaporator working with a R1234ze(E) refrigerant. The results from both studies will be then compared for several similar configurations, to confirm the transferability of the main conclusions of the present article to an actual evaporator and refrigerant flow. Besides, thanks to such DOE study, an interpolating equation that relates the comparative response variable (i.e. STD_{water} in the present case) to the parameters involved can be obtained. This equation can be then further used to predict the performances of the combination of parameters that have not been tested in the test matrix [31]. Such predictive equation is usually the objective of a DOE study. However, in the present work, 48 tests were not sufficient to obtain a sufficiently accurate equation. This is mainly because the physical forces driving the two-phase flow distribution are so different according to the header and channel orientation, that much more than 12 tests per orientation would be needed to characterize the distribution accurately. For instance, Tempesti et al. with 72 tests over a total of 108 performed only in a HH-VDC orientation and with a 23 mm inlet tube diameter, managed to obtain a predictive model of 51% of accuracy. Thereby, the minimum amount of tests required to reach an acceptable accuracy of the predictive equation would have been tremendous for the present work. Finally, in a future work, the combination of parameters identified from the DOE mean plot in the Section 5.1.2 could be tested, to confirm this result.

Declaration of competing interest

The authors declare that they have no known competing financial interests or personal relationships that could have appeared to influence the work reported in this paper.

Acknowledgments

This project has received funding from the Clean Sky2 Joint Undertaking (JU) under grant agreement No 886698. The JU receives support from the European Union's Horizon 2020 research and innovation programme and the Clean Sky 2 JU members other than the Union. This paper reflects only the author's view and that the JU is not responsible for any use that may be made of the information it contains. The work presented is part of the PANTTHER project results, funded by LIEBHERR Aerospace and the EU. The authors would like to thank the funders for their financial support, which made this project possible.

Data availability

The authors do not have permission to share data.

References

[1] G. Falcone, G.F. Hewitt, C. Alimonti, Multiphase Flow Metering - Pinciple and Applications, Elsevier, 2010.
[2] Julio C. Pacio, Carlos A. Dorao, A study of the effect of flow maldistribution on heat transfer performance in evaporators, Nucl. Eng. Des. (ISSN: 00295493) 240 (2010) 3868–3877, http://dx.doi.org/10.1016/j.nucengdes.2010.09.004.
[3] J. Choi, William Payne, Piotr Domanski, Effects of non-uniform refrigerant and air flow distributions on finned-tube evaporator performance, in: Refrigeration International Congress, 21st IIR. (IRC2003). 10th Technical Session Energy-Efficient Heating and Cooling Systems for Buildings. Proceedings. August 17-22, 2003, Washington, DC, USA, 2003, URL https://tsapps.nist.gov/publication/get_pdf.cfm?pub_id=101203.
[4] E.R. Dario, L. Tadrist, J.C. Passos, Review on two-phase flow distribution in parallel channels with macro and micro hydraulic diameters: Main results, analyses, trends, Appl. Therm. Eng. 59 (1–2) (2013) 316–335.
[5] Tong Xiong, Guoqiang Liu, Shenjie Huang, Gang Yan, Jianlin Yu, Two-phase flow distribution in parallel flow mini/micro-channel heat exchangers for refrigeration and heat pump systems: A comprehensive review, Appl. Therm. Eng. 201 (2022) 117820.
[6] Sang Yong Lee, Flow distribution behavior in condensers and evaporators, in: International Heat Transfer Conference 13, Begel House Inc., 2006.
[7] J.K. Lee, S.Y. Lee, Distribution of two-phase annular flow at header-channel junctions, Exp. Therm. Fluid Sci. 28 (2004) 217–222.
[8] J.K. Lee, Study on Effect of Channel Intrusion Depth on the Two-Phase Flow Distribution at Header-Channel Junction, Korean J. Air-Conditioning Refrig. Eng. 28 (11) (2016) 444–449.
[9] P. Fei, P. Hrnjak, Adiabatic Developing Two-Phase Refrigerant Flow in Manifolds of Heat Exchangers, TR-225, Air Condtioning and Refrigeration Center, 2004.
[10] S. Vist, J. Pettersen, Two-phase flow distribution in compact heat exchanger manifolds, Exp. Therm. Fluid Sci. 28 (2004) 209–215.
[11] Honggi Cho, Keumnam Cho, Mass flow rate distribution and phase separation of R-22 in multi-microchannel tubes under adiabatic condition, Microscale Thermophys. Eng. 8 (2) (2004) 129–139.

[12] N.-H. Kim, D.-Y. Kim, H.-W. Byun, Effect of inlet configuration on the refrigerant distribution in a parallel flow minichannel heat exchanger, Int. J. Refrig. 34 (2011) 1209–1221.
[13] E.R. Dario, L. Tadrist, J.L.G. Oliveira, J.C. Passos, Measuring maldistribution of two-phase flows in multi-parallel microchannels, Appl. Therm. Eng. 91 (2015) 924–937.
[14] H.W. Byun, N.H. Kim, Refrigerant distribution in a parallel flow heat exchanger having vertical headers and heated horizontal tubes, Exp. Therm. Fluid Sci. 35 (6) (2011) 920–932.
[15] Nae-Hyun Kim, Tae-Ryong Sin, Two-phase flow distribution of air–water annular flow in a parallel flow heat exchanger, Int. J. Multiph. Flow 32 (12) (2006) 1340–1353.
[16] Y. Hwang, D.-H. Jin, R. Radermacher, Refrigerant Distribution in Minichannel Evaporator Manifolds, HVACR Res. 13 (4) (2007) 543–555.
[17] J.K. Lee, The Effect of Header and Channel Angle Variation on Two-Phase Flow Distribution at Multiple Junctions, Korean J. Air-Conditioning Refrig. Eng. 27 (11) (2015) 559–566.
[18] F. Poggi, Etude de la Distribution D'écoulements Mono- et Diphasiques Dans un Échangeur à Mini-Canaux. pertes de Pression Régulières et Singulières (Ph.D. thesis), Université Joseph Fourier, Grenoble, France, 2008.
[19] T. Yoo, P. Hrnjak, T. Newell, An Experimental Investigation of Two-phase Flow Distribution in Microchannel Manifolds, Technical Report TR-207, Air Conditioning and Refrigeration Center, University of Illinois at Urbana-Champaign, 2002.
[20] M. Ahmad, G. Berthoud, P. Mercier, General characteristics of two-phase flow disitrbution in a compact heat exchanger, Int. J. Heat Mass Transfer 52 (2009) 442–450.
[21] M. Ahmad, Etude Expérimentale et Numérique d'Écoulements Diphasiques à L'entrée des Évaporateurs de Cycles Thermodynamiques (Ph.D. thesis), Institut National Polytechnique de Grenoble, 2007.
[22] Q. Zhang, P. Hrnjak, T. Newell, An Experimental Investigation of R134a Flow Distribution in Horizontal Microchannel Manifolds, TR-223, Air Conditioning and Refrigeration Center, 2003.
[23] Yang Zou, Pega S. Hrnjak, Effects of fluid properties on two-phase flow and refrigerant distribution in the vertical header of a reversible microchannel heat exchanger–Comparing R245fa, R134a, R410a, and R32, Appl. Therm. Eng. 70 (1) (2014) 966–976.
[24] R.L. Webb, K. Chung, Two-Phase Flow Distribution to Tubes of Parallel Flow Air-Cooled Heat Exchangers, Heat Transf. Eng. 26 (4) (2005) 003–018.
[25] Ian H. Bell, Jorrit Wronski, Sylvain Quoilin, Vincent Lemort, Pure and Pseudo-pure fluid thermophysical property evaluation and the Open-Source thermophysical property library CoolProp, Ind. Eng. Chem. Res. 53 (6) (2014) 2498–2508, http://dx.doi.org/10.1021/ie4033999, URL http://pubs.acs.org/doi/abs/10.1021/ie4033999.
[26] R. Massoudi, A.D. King Jr., Effect of pressure on the surface tension of water. Adsorption of low molecular weight gases on water at 25. deg., J. Phys. Chem. 78 (22) (1974) 2262–2266.
[27] J.K. Lee, Two-phase flow behavior inside a header connected to multiple parallel channels, Exp. Therm. Fluid Sci. 33 (2009) 195–202.
[28] ISO 5167-4:2003, Measurement of Fluid Flow by Means of Pressure Differential Devices Inserted in Circular Cross-Section Conduits Running Full, Part 4: venturi Tubes, Standard, International Organization for Standardization, Geneva, CH, 2003.
[29] Aude Lecardonnel, Carlo De Servi, Piero Colonna, Delphine Laboureur, Two-phase flow metering of maldistribution inside a header by means of venturi flowmeter solely, Multiph. Sci. Technol. 36 (1) (2024).
[30] Douglas C. Montgomery, Design and Analysis of Experiments, ISBN: 9781118146927.
[31] Claretta Tempesti, Aude Lecardonnel, Delphine Laboureur, Experimental assessment of multi-phase flow distribution in an evaporator header through Design of Experiments techniques, Exp. Therm. Fluid Sci. 162 (2025) 111359.
[32] DoEgen python package, 2021, https://pypi.org/project/DoEgen/. (Accessed 11 2021 12 2021).
[33] Ovid Baker, Design of pipelines for the simultaneous flow of oil and gas, in: SPE Annual Technical Conference and Exhibition?, SPE, 1953, pp. SPE–323.
[34] Bamdad Salemi, Contributions Expérimentales sur les Écoulements Diphasiques Dans un Évaporateur de Climatisation: Essais en Eau-Air et en Réfrigérant R134a (Ph.D. thesis), Université de Lorraine, 2014.
[35] Agung Tri Wijayanta, Takahiko Miyazaki, Shigeru Koyama, Refrigerant distribution in horizontal headers with downward minichannel-branching conduits: Experiment, empirical correlation and two-phase flow pattern map, Exp. Therm. Fluid Sci. 81 (2017) 430–444.
[36] ZM Razlan, SA Bakar, H Desa, WK Wan, I Zunaidi, I Ibrahim, NS Kamarrudin, MJM Ridzuan, K Takiguchi, T Tsuchiya, et al., Experimental study on gas–liquid flow distributions in upward multi-pass channels—Comparison of R-134a flow and air–water flow, Exp. Therm. Fluid Sci. 91 (2018) 134–143.
[37] Geoffrey Frederick Hewitt, D.N. Roberts, Studies of Two-Phase Flow Patterns by Simultaneous X-Ray and Flast Photography, Technical Report, Atomic Energy Research Establishment, Harwell, England (United Kingdom), 1969.
[38] Lixin Cheng, Gherhardt Ribatski, John R. Thome, Two-phase flow patterns and flow-pattern maps: fundamentals and applications, 2008.
[39] Dvora Barnea, A unified model for predicting flow-pattern transitions for the whole range of pipe inclinations, Int. J. Multiph. Flow 13 (1) (1987) 1–12.
[40] Jun Kyoung Lee, Optimum channel intrusion depth for uniform flow distribution at header-channel junctions, J. Mech. Sci. Technol. 24 (2010) 1411–1416.
[41] Mark Anthony Redo, Jongsoo Jeong, Niccolo Giannetti, Koji Enoki, Seiichi Yamaguchi, Kiyoshi Saito, Hyunyoung Kim, Characterization of two-phase flow distribution in microchannel heat exchanger header for air-conditioning system, Exp. Therm. Fluid Sci. 106 (2019) 183–193.
[42] Yang Zou, Pega S. Hrnjak, Experiment and visualization on R134a upward flow in the vertical header of microchannel heat exchanger and its effect on distribution, Int. J. Heat Mass Transfer 62 (2013) 124–134.
[43] Ho-Won Byun, Nae-Hyun Kim, Two-phase refrigerant distribution in an intermediate header of a parallel flow minichannel heat exchanger, Int. J. Refrig. 59 (2015) 14–28.
[44] Nae-Hyun Kim, Ho-Won Byun, Yong-Sub Sim, Upward branching of two-phase refrigerant in a parallel flow minichannel heat exchanger, Exp. Therm. Fluid Sci. 51 (2013) 189–203.